Marine and Petroleum Geology 146 (2022) 105936

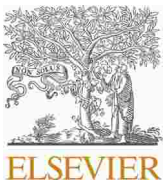

Contents lists available at ScienceDirect

Marine and Petroleum Geology

journal homepage: www.elsevier.com/locate/marpetgeo

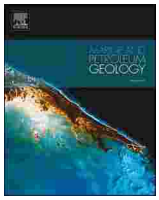

Modelling of pore pressure evolution in a compressional tectonic setting: The Kuqa Depression, Tarim Basin, northwestern China

Bing Wang [a,b,c], Nansheng Qiu [a,b,*], Sebastian Amberg [c], Yunjiang Duan [d], Ralf Littke [c]

[a] College of Geosciences, China University of Petroleum, 102249, Beijing, China
[b] State Key Laboratory of Petroleum Resources and Prospecting, China University of Petroleum, 102249, Beijing, China
[c] Energy & Mineral Resources Group (EMR), Institute of Geology and Geochemistry of Petroleum and Coal, RWTH Aachen University, 52064, Aachen, Germany
[d] Exploration and Development Research Institute, PetroChina Tarim Oilfield Company, 841000, Korla, China

ARTICLE INFO

Keywords:
Fluid overpressure
Tectonic compression
Salt cap rock
Basin and petroleum system modelling
Kuqa depression

ABSTRACT

The Kuqa Depression is part of a Mesozoic-Cenozoic foreland basin located at the northern margin of the Tarim Basin. High fluid overpressures were reported in the Mesozoic section related to both the complex tectonic evolution and the sealing by the salt-bearing sequence within the Paleogene Kumugeliemu Group. The role of structural evolution and compressional shortening in the generation of overpressures is poorly understood and requires a model-based understanding of the basin structure for different time steps. Structurally restored geometries based on a present-day geological section interpreted from a 2D seismic line, has been used as input for a basin and petroleum system model to simulate pore pressure history through geological time. In this simulation, we demonstrate structural dependencies of pore pressure development, and examine the impact of disequilibrium compaction, tectonic compression, opening and closing of faults over time, as well as folding on overpressure evolution. The poroelastic model is used to quantitatively evaluate the contribution of horizontal shortening due to tectonic compression on overpressure. We found that the pressure increase caused by 12.5% shortening can account for a maximum of more than 60% of overpressure, depending on lithology and deformation strength. We also simulated the effect of salt content within the seal layer on overpressure and found that the increase in salt has promoted the onset time and magnitude of overpressure in the underlying strata, which favors porosity preservation. A heat flow sensitivity analysis was performed, suggesting that the pressure increase caused by extremely high heat flow is rather low.

1. Introduction

High pore pressures are observed in the subsurface of the Kuqa Depression and commonly occur in areas with strong tectonic activity and complex structures (Berry, 1973; Grauls and Baleix, 1994; Fisher and Zwart, 1996; Zhang et al., 2021). Overpressure plays an important role in many geological processes in sedimentary basins, influencing hydrocarbon migration (England et al., 1987), reservoir properties (Swarbrick, 2002), the integrity of seal rocks (Nordgård-Bolås et al., 2005; Webster et al., 2011), and basin evolution (Hubbert and Rubey, 1959; Brown and Karim, 2008). In addition, the prediction of overpressure is important to reduce the cost and risk of drilling (Zoback, 2007). Basin and petroleum system modelling (BPSM) is an important method to quantitatively restore pore pressure and distribution through geological time by combining key geological elements in basin history (Luo and Vasseur, 1995; Hantschel and Kauerauf, 2009; Neumaier et al., 2014).

The Kuqa Depression has become the origin of China's west-east gas transmission project with the discovery of a number of large and medium-sized oil and gas fields since the exploration in the 1990s (Jia and Li, 2008; Fan et al., 2021). The area has experienced increasing tectonic compression since the Neogene, the timing and magnitude of overpressure varying throughout the basin, depending on the local tectonic history (Lu et al., 1997; Allen et al., 1999). Disequilibrium compaction related to rapid deposition and low permeability rock was considered one of the main causes of overpressure in the study area (Jia and Li, 2008). Furthermore, tectonic compression significantly increased pore pressure in a similar way as disequilibrium compaction, in which horizontal stress causes further compaction and a decrease in permeability, thereby resulting in retardation of fluid expulsion and

* Corresponding author. State Key Laboratory of Petroleum Resources and Prospecting, China University of Petroleum, 102249, Beijing, China.
E-mail address: qiunsh@cup.edu.cn (N. Qiu).

https://doi.org/10.1016/j.marpetgeo.2022.105936
Received 18 May 2022; Received in revised form 19 September 2022; Accepted 20 September 2022
Available online 24 September 2022

overpressure generation (Zeng et al., 2010; Guo et al., 2016a, 2016b). Hydrocarbon generation may also make some contribution (Zeng and Liu, 2006). Present-day closed thrust faults separate the basin into many isolated pressure systems and prevent hydrocarbon leakage (Zhou, 2001; Fu et al., 2015; Guo et al., 2016c). The preservation of strong overpressure is closely linked to the regional salt-bearing seal rocks, in which near-lithostatic pressures have been encountered in highly deformed areas (Zhou, 2001; Pi et al., 2002; Jia and Li, 2008). Even though these studies mentioned above suggest that the development and distribution of pore pressure in the Kuqa Depression are the results of the interaction of many factors, a simulation that is capable of coupling various overpressure mechanisms are missing, especially for the dynamic process of overpressure evolution in response to tectonic event through geologic time. The traditional basin models applied in the Kuqa Depression only considered overburden loading based on Terzaghi theory (Shi, 2008; Wang et al., 2016; Wan et al., 2021), which neglects the impact of horizontal shortening on pore pressure.

This study aims to provide a deep understanding of how pore pressures evolved under the control of tectonic history in the Kuqa Depression by combining structural reconstruction and basin and petroleum system modelling, coupling the effect of overburden load, tectonic compression, salt seal, faults and folds on pore pressure during the basin evolution. Finally, the contribution of tectonic compression and salt seal to overpressures, two potentially important factors, are quantitatively evaluated.

2. Geological setting

2.1. Structure and stratigraphy

The Tarim Basin in northwestern China is bounded by the Kunlun-Altun Mountains in the south and the Southern Tianshan Mountains in the north. The Kuqa Depression is located north of the Tarim Basin, bordered by the South Tianshan Mountains in the north and the northern uplift in the south. The Kuqa Depression can be further divided into four structural belts and three sags from north to south, including the northern monoclinal belt, Kelasu-Yiqikelike structural belts, Wushi-Baicheng-Yangxia sags, Qiulitage structural belt and southern slope belt (Jia and Li, 2008, Fig. 1). The Kelasu-Yiqikelike and Qiulitage structural belts are the main oil and gas producing areas, where hydrocarbons are mainly stored in structural traps (Zhu et al., 2015).

The Kuqa Depression is part of a foreland basin filled by Mesozoic-Cenozoic sediments, overlying the peripheral foreland basin formed from Permian times to the end of the Early Triassic. It experienced an extensional stage during the Late Triassic through the Paleogene and a rejuvenated foreland basin stage since the Neogene (Graham et al., 1993; Lu et al., 1997; Zeng et al., 2010). Due to the southward-compression of the Southern Tianshan Mountains in the Middle and Late Himalayan periods, the structural belts in the Kuqa Depression formed from north to south successively (Yin et al., 1998; Wang et al., 2004). The initial tectonic deformation occurring in the Early Miocene resulted in the formation of the northern monoclinal belt; the formation of the Kelasu-Yiqikelike structural belts began in the Late Miocene, and the Qiulitage structural belt started to form in the Early

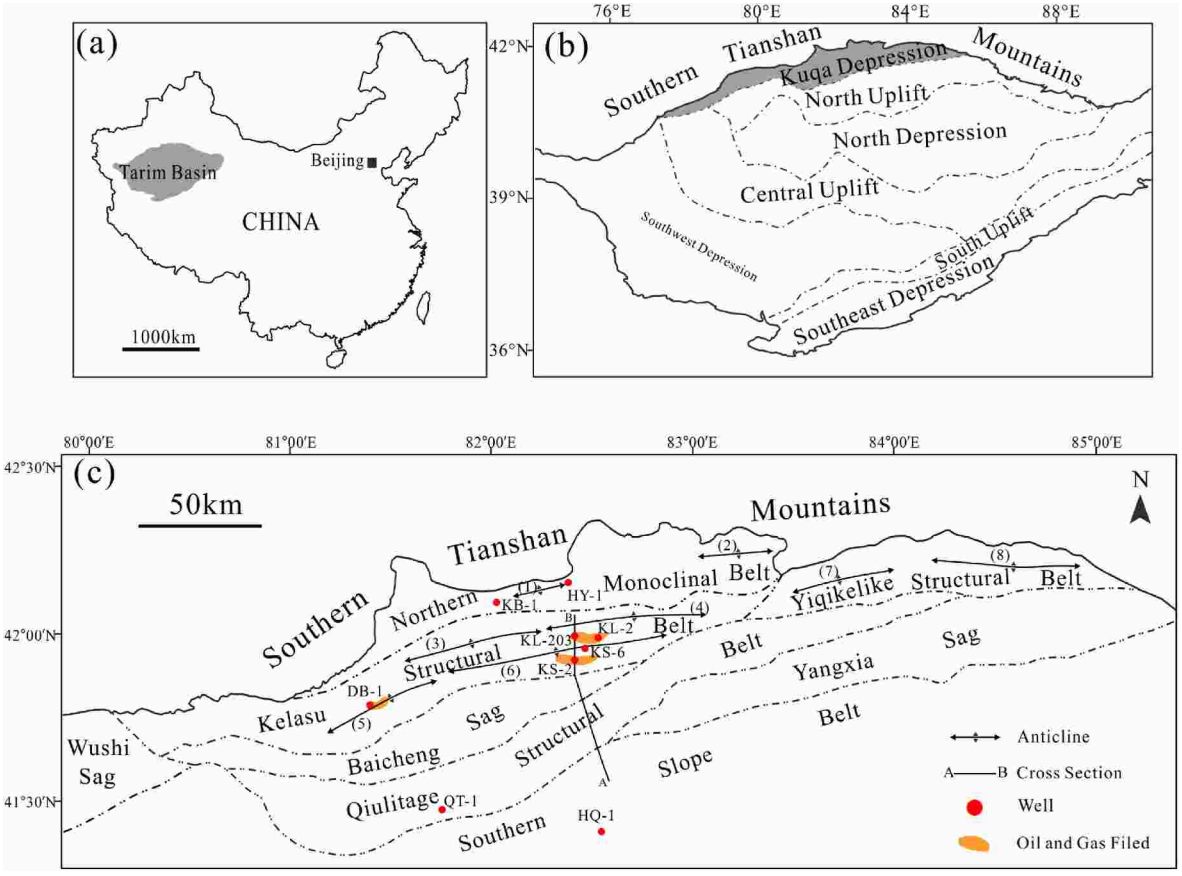

Fig. 1. (a) Geographic location of the Tarim Basin in northwestern China. (b) Map showing the tectonic units of the Tarim Basin and location of the Kuqa Depression (modified after Fan et al., 2021). (c) Tectonic map of the Kuqa Depression adjacent to the Southern Tianshan Mountains (modified after Li et al., 2012; Guo et al., 2016a), showing secondary tectonic units, representative wells, major anticlines, and seismic line A-B. Numbers (1) to (8) represent the names of the anticlines: (1) Bashikutan anticline, (2) Jiesidelike anticline, (3) Kumugeliemu anticline, (4) Bashijiqike anticline, (5) Tuzimazha anticline, (6) Kasangtuokai anticline, (7) Yiqikelike anticline, (8) Tugerming anticline.

Pliocene. In the Late Pliocene, the uplift of the Tianshan Mountains and crustal shortening accelerated and the previously formed structural belts were further consolidated, subsequently leading to strong erosion (Tang et al., 2004). During the Quaternary period, a large amount of sediments was deposited in structurally low parts of the Kuqa Depression (Li et al., 2012). Controlled by compressional tectonics and the resulting lithosphere thickening over time, the heat flow in the study area gradually decreased during the Cenozoic, and the present-day heat flow is predicted to be as low as about 40 mW/m^2 (Li et al., 2010; Qiu et al., 2012; Tang et al., 2014).

The strata in the Kuqa Depression comprise the Triassic-Quaternary sediments (Fig. 2). During the Triassic to the Middle Jurassic, lacustrine, swamp-lake transitional and delta-swamp alternating sediments were deposited successively (Huang et al., 2019). The main petroleum source rocks are lacustrine mudstones within the Upper Triassic Taliqike Formation as well as carbonaceous mudstones and lacustrine mudstones in the Lower Jurassic Yangxia Formation and the Middle Jurassic Kizilenur Formation (Zhao et al., 2005). Potential reservoirs of conglomerate-bearing sandstones were deposited in a braided river delta setting during the Early Jurassic (Ahe Formation; Liang et al., 2003). Sediments of shallow lacustrine and fan delta facies developed during the Late Jurassic and Early Cretaceous, with sandstones comprising the dominant lithology in the Lower Cretaceous sequence. The absence of the upper Cretaceous is due to regional tectonic uplift and erosion (Jia and Li, 2008; Wang et al., 2011). The sandstone units in the Lower Cretaceous Bashijiqike Formation, combined with conglomerate-bearing sandstones at the base of the Paleogene Kumugeliemu Group, form another excellent reservoir unit in the Kuqa Depression (Zeng et al., 2010; Fan et al., 2021). The Kumugeliemu Group is usually divided into four members based on lithology, in which the salt-bearing mudstone units in the second member provide an important regional seal. It is worth noting that the main petroleum-producing layers are the Bashijiqike Formation and the Member 4 of the Kumugeliemu Group (conglomerate-bearing sandstone at the base of the Kumugeliemu Group mentioned above) in the Kelasu and Qiulitage structural belts, and the Ahe Formation in the Yiqikelike structural belt, where the Mesozoic is at lower present-day burial depth because of strongly eroded Cenozoic strata (Guo et al., 2016a).

Influenced by the salt-bearing ductile layer in the Member 2 of the Kumugeliemu Group, the deformation characteristics of the sections above and below this layer are quite different, although they experienced the same tectonic evolution. Thrust faults and fault-related folds formed above the ductile layer, while typical imbricated structures, comprised of thrust slices in the Mesozoic strata, were developed below the ductile layer in which the thrust faults terminate upward (Tang et al., 2004; Jia and Li, 2008). Due to the combined effects of tectonic compression and overburden loading, the thickness of the Member 2 of the Kumugeliemu Group varies greatly throughout the Kuqa Depression due to its ductile nature.

2.2. Pore pressure characteristics at the present day

Because almost all measured data from drill stem tests (DSTs) are distributed in the reservoir rocks only, such as in the Bashijiqike Formation and the Member 4 of the Kumugeliemu Group, mud weights are used as a proxy for pore pressure to obtain the characteristics of pressure variation with depth in the Kuqa Depression, although mud weight is commonly not exactly equal to the pore pressure. Given that density log operations for most wells in this area are confined to the petroleum-producing intervals, instead, sonic log data are utilized to calculate porosity (Schlumberger, 1989) to reflect the distribution of porosity along depth. It should be noted that mud weight used as a proxy should be treated with caution. This is because the mud weight is not considered a reliable indicator in intervals with unbalanced drilling (Webster et al., 2011). In addition, acoustic data should be treated carefully because they are sometimes affected by unfavorable borehole conditions and cement types (Tingay et al., 2013). Nevertheless, mud weights and sonic log data can provide at least a general guide for the trend of pore pressure and porosity with depth, respectively (Webster et al., 2011).

Pressure- and porosity-depth plots are presented for five representative wells from different structural belts (Fig. 3), which show variable characteristics of pore pressure across different structural belts. The overpressured intervals are identified by a significant increase in mud weight, measured pressure, and abnormally high porosities. The tops of overpressure in the KS-2 and KS-6 wells in the Kelasu structural belt are located within the Kumugeliemu Group. Within the Kumugeliemu Group, a rapid increase in overpressure to near lithostatic pressure is observed, associated with the high sealing effectiveness of salt. The overpressures slightly decreased in the Bashijiqike Formation with measured overpressures of 54.1 MPa and 43.8 MPa in the KS-2 and KS-6 wells, respectively. The distribution of abnormally high porosity is consistent with overpressure intervals. Overpressure in the QT-1 well in the Qiulitage structural belt commences in the Jidike Formation, with a lower measured overpressure of 20.6 MPa. It is assumed that the KB-1 well in the northern monoclinal belt may develop weak overpressures only, near hydrostatic values, because of the measured overpressure of only 3.1 MPa at a burial depth of 3682 m. However, undercompaction in the porosity-depth plot is observed. In addition, the fact that mud losses occurred a dozen times when using mud with a density of 1.25–1.37 g/cm^3 in the sequences below the Bashijiqike Formation (according to the unpublished drilling logs provided by Tarim Oilfield Company) indicates that mud weight is much greater than pore pressure in the KB-1 well. The HQ-1 well, located in the southern slope belt, has no overpressure based on all observations including measured pressure, the trend of mud weight and porosity with depth.

3. Structural restoration

3.1. Selected seismic section

The south-north seismic section (A-B) has been selected to construct a basin and petroleum system model (see Fig. 1c for location). This section intersects the Kelasu structural belt, Baicheng sag, Qiulitage structural belt, and southern slope belt from north to south and passes through the KL-203 and KS-2 wells in the Kelasu structural belt. It crosscuts several important structural elements and is thus a good representation of the tectonic evolution and sedimentary history of the Kuqa Depression, where tectonic extension and compression occurred successively since the Late Triassic. Horizons and faults in the seismic section were based on the interpretation from the unpublished research report by Shi and Qi (2015; Fig. 4). However, poor-quality seismic data have led to uncertain interpretations at some locations, particularly those experiencing large burial depth or/and complex structural deformation. The section has been divided vertically into three tectonic sequences according to deforming characteristics: the supra-salt sequence, the salt-bearing sequence (Kumugeliemu Group) and the sub-salt sequence. The Bashijiqike anticline (BS), Kasangtuokai anticline (KA), Baicheng sag (BS), and Qiulitage anticline (QA) are identified in this section from north to south.

3.2. Structural restoration method

A reasonable paleo-geometry at each geological time is the backbone of 2D basin and petroleum system modelling. As previously mentioned, the Kuqa Depression experienced extensional tectonics during the Late Triassic through the Paleogene and a compressional rejuvenated foreland basin stage since the Neogene. Therefore, in the first stage when rocks moved mainly in vertical direction, backstripping approach has been applied for the restoration of paleo-geometries, which considers decompaction, erosion and paleo thickness corrections. Herein, the erosion restoration was implemented during the Late Cretaceous period, based on the erosion map reported by Yu et al. (2016). Yu et al. (2016)

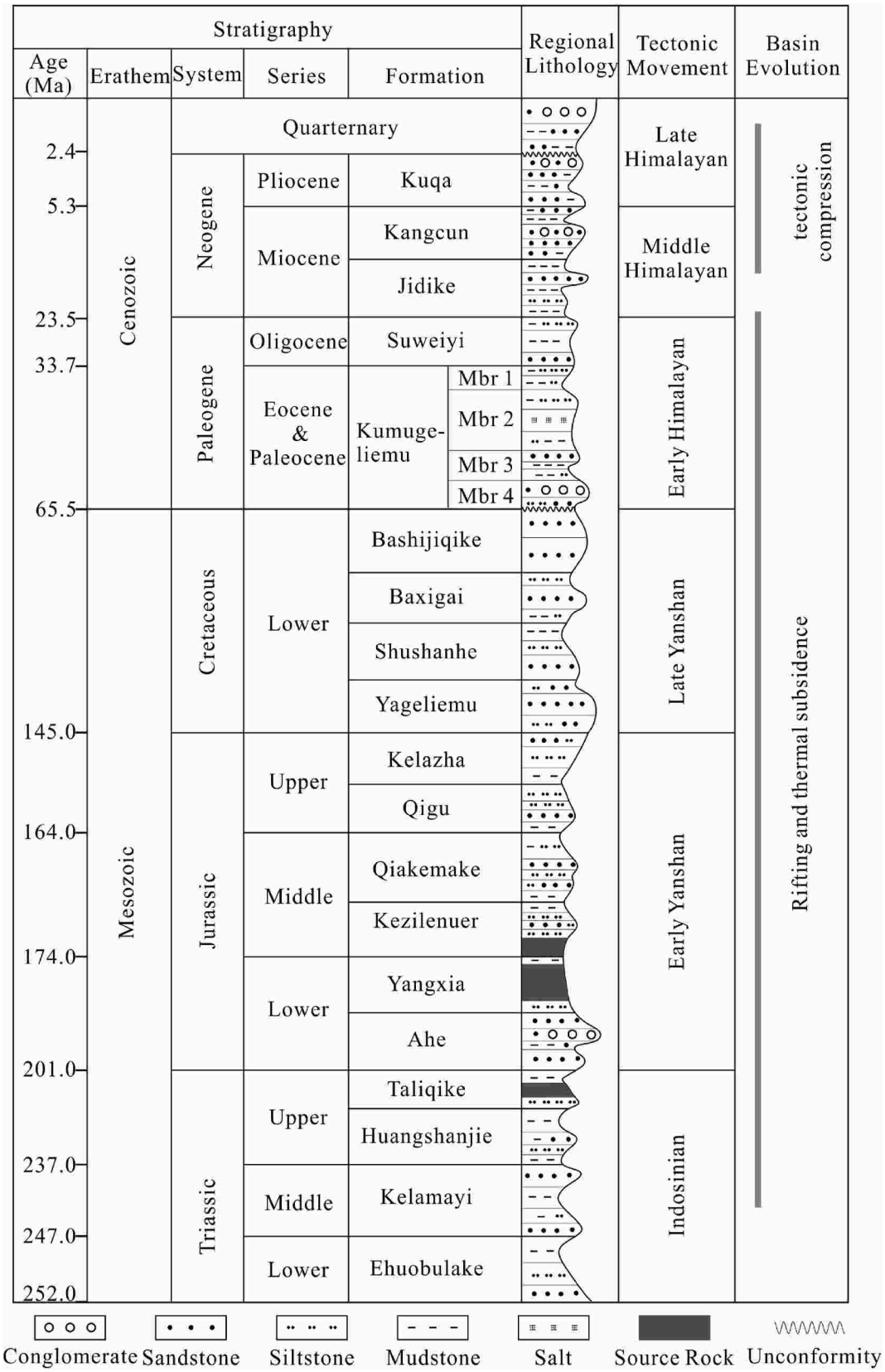

Fig. 2. Lithostratigraphy of the Kuqa Depression (modified after Guo et al., 2016a), showing lithology in each formation, major tectonic events and basin evolution. Mbr = Member.

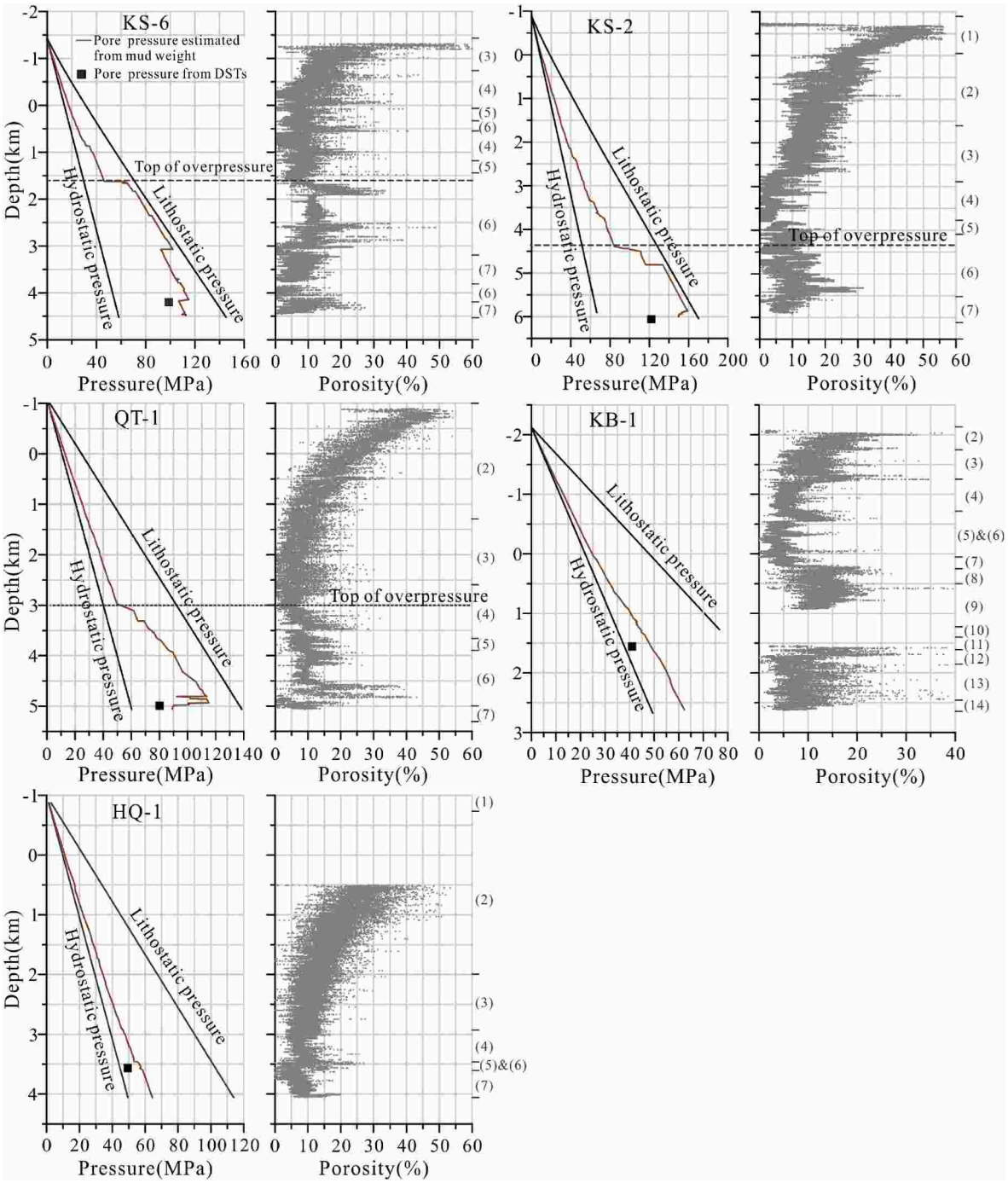

Fig. 3. Pressure and porosity distribution in wells KS-6, KS-2, QT-1, KB-1, HQ-1. The depths of all wells are referenced to sea level. The left panel of each well shows pressure distribution based on mud weight (brown curved line) and drill stem tests (square), and calculated litholostatic and hydrostatic pressure. Dashed line represents the top of overpressure. The right panel shows porosity distribution estimated from acoustic logs (dots). KS-6, KS-2 and QT-1 have overpressures, while only weak overpressures or hydrostatic pressures are developed in KB-1 and HQ-1. See Fig. 1 for well locations. (1) = Quaternary; (2) = Kuqa Formation; (3) = Kangcun Formation; (4) = Jidike Formation; (5) = Suweiyi Formation; (6) = Kumugeliemu Group; (7) = Bashijiqike Formation; (8) = Baxigai Formation; (9) = Shushanhe Formation; (10) = Yageliemu Formation; (11) = Qigu Formation; (12) = Qiakemake Formation; (13) = Kezilenuer Formation; (14) = Yangxia Formation. (For interpretation of the references to colour in this figure legend, the reader is referred to the Web version of this article.)

approximated the location of the subsidence center prior to the Late Cretaceous erosion based on seismic, logging and drilling data. According to this data and interpretation, the original depositional thickness (i.e., the stratigraphic thickness prior to erosion) of the Cretaceous decreased gradually from the subsidence center to the north and south sides. Yu et al. (2016) had two basic assumptions: 1) the Cretaceous stratigraphy was not eroded in the subsidence center, where the present-day thickness is the original deposited one; 2) the "thinning rate" (i.e., the horizontal decrement of the deposition thickness per unit distance) of the original sedimentary stratigraphy away from the subsidence center is uniform, which is acceptable, because the weak tectonic activity during the Cretaceous period allowed for a relatively flat topography and resulted in strata with a progressive thickness decrease. Thinning rates based on seismic and well data were combined with the thickness of deposited sediments in the subsidence center and thus the distribution of the original depositional thickness was extrapolated for

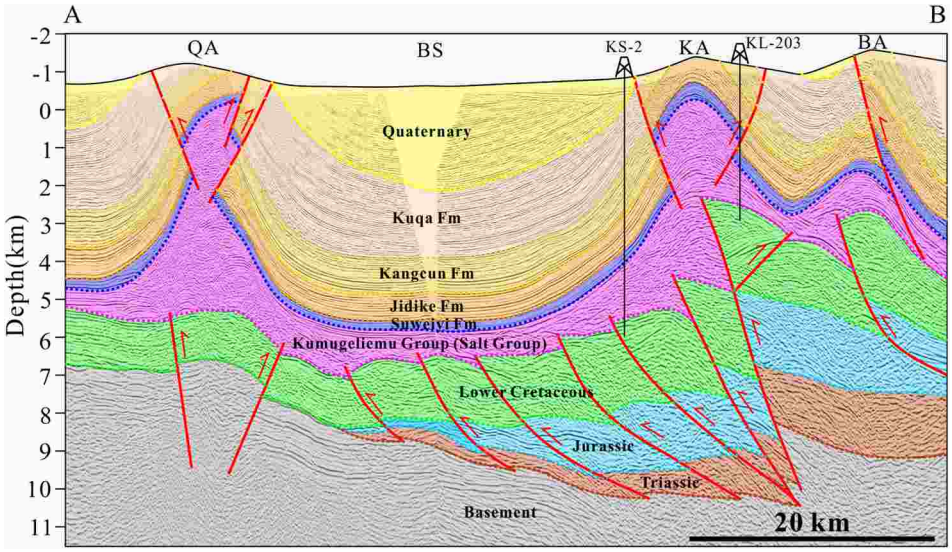

Fig. 4. Interpreted 2-D seismic line across wells KS-2 and KL-203 in the Kuqa Depression (see Fig. 1 for location). BA=Bashijiqike anticline; KA=Kasangtuokai anticline; QA = Qilitage anticline; BS=Baicheng sag. The seismic interpretation is based on the unpublished research report by Shi and Qi (2015).

the entire study area. Finally, an erosion map was obtained by subtracting the residual stratigraphic thickness at the present day from the original depositional thickness. In addition, given that terrestrial sediments dominated during this stage and paleo-water depths of only a few or tens of meters are negligible relative to the model thickness, the top horizon of paleo-geometry is set to sea level.

However, for the rejuvenated foreland basin stage, the classical backstripping method is unable to account for lateral deformation and movement of rocks, thereby creating geologically unreasonable paleo-geometries (Neumaier et al., 2014). Instead, geomechanics-based structural restoration has been performed using a finite element method-based tool, the Dynel 2D, to reconstruct complex tectonic history in the rejuvenated foreland basin stage. This tool uses physical principles of the conservation of mass and momentum and linear-elastic theory to control rock deformation and movement (Maerten and Maerten, 2006). Structurally reconstructed models go backwards in time from a present-day geometry by removing sequentially older sediment layers, restoring faults, unfolding structural deformation and decompacting the underlying sediments at each successive time step (Hantschel and Kauerauf, 2009). However, due to the highly ductile nature of salt, deformation of salt-bearing layers is characterized by plastic flow and is significantly driven by kinematic behaviors of both supra-and sub-salt sequences during tectonic compression (Gemmer et al., 2004). This type of kinematic behavior commonly results in an irregular deformation and laterally varying thickness of the salt-bearing layer, which makes structural restoration a great challenge. Considering the highly ductile nature of salt and the occurrence of salt flow during tectonic compression, we employed the following method to obtain the paleo-geometry of the salt-bearing layer indirectly: first, the salt-bearing layer was removed from the model, and then supra- and sub-salt sequences were structurally restored separately. To model salt flow during restoration, the top and base of the salt-bearing layer (i.e., the base of the supra-salt sequence and the top of the sub-salt sequence, respectively) remain free to move in vertical and horizontal directions. In this way, the restored deformation of the salt-bearing layer mainly depends on the structural restoration of both supra- and sub-salt sequences. Finally, the restored space between the base of the supra-salt sequence and the top of the sub-salt sequence is considered as the paleo-geometry of the salt-bearing layer and was then filled with the corresponding salt-bearing lithology. Any freshly created space between this base and top during restoration represents the restored deformation amount of the salt-bearing layer (Schultz-Ela, 1992; Allwardt et al., 2009). Hence, the change in the salt-bearing layer area indicates the inflow or outflow of rocks in the section. Besides, to adequately demonstrate the relationship between folding and pressuring, an additional time step at 2.0 Ma has been added, in which the Qiulitage anticline had formed, and the surfaces of the anticlines of BashiJiqike and Kasangtuokai had been eroded to varying degrees.

During structural restoration, some boundary conditions need to be set. The south (i.e., left) boundary of the geometry is fixed in the horizontal direction, and the north (i.e., right) boundary can move freely. In order to describe the compression process, lateral displacement on the boundary walls or sides of the structure is imposed to pull back thrust or fold structures effectively. The model surface is considered free in the vertical direction, and its altitude is determined by unfolding, unfaulting and restoring erosion.

4. Model construction and results

4.1. Paleo-geometries based on structural restoration

In the following section, structural restoration results are described for the last 17 Ma, i.e., since the Miocene (Fig. 5). Basin history from the Late Triassic to Paleogene (240–16.9 Ma) reconstructed by backstripping approach is not the focus of our study and thus not be shown, even though it has been incorporated into the basin model. At the end of the Jidike Formation deposition (16.9 Ma; Fig. 5a), only weak deformation of rocks took place due to the compression of the Southern Tianshan mountains at the northern margin. During the Kangcun Formation deposition (16.9–5.3 Ma; Fig. 5b), deformation continued to spread southward with increasing compression, and the Bashijiqike and Kasangtuokai anticlines began to develop in the Kelasu structural belt. The Kumugeliemu Group (Salt Group) visibly thickened associated with the start of plastic flow due to tectonic compression. During the Kuqa Formation deposition (5.3–2.4 Ma; Fig. 5c), the Qiulitage anticline formed, and the other two anticlines were further enhanced with the initiation of two thrust faults, F15 and F17. At 2.0 Ma (Fig. 5d), the three anticlines became even more deformed, and the Baicheng sag was built, accompanied by the occurrence of more thrust faults within sequences above and below the Kumugeliemu Group (Salt Group). The Kuqa Formation at the top of anticlines was partially eroded. A thrust-imbricated structure was developed to the south of the F15 fault, and back-thrust and anti-thrust structures to the north. From 2.0 Ma through 1.75 Ma (Fig. 5e), the central section experienced varying amounts of burial,

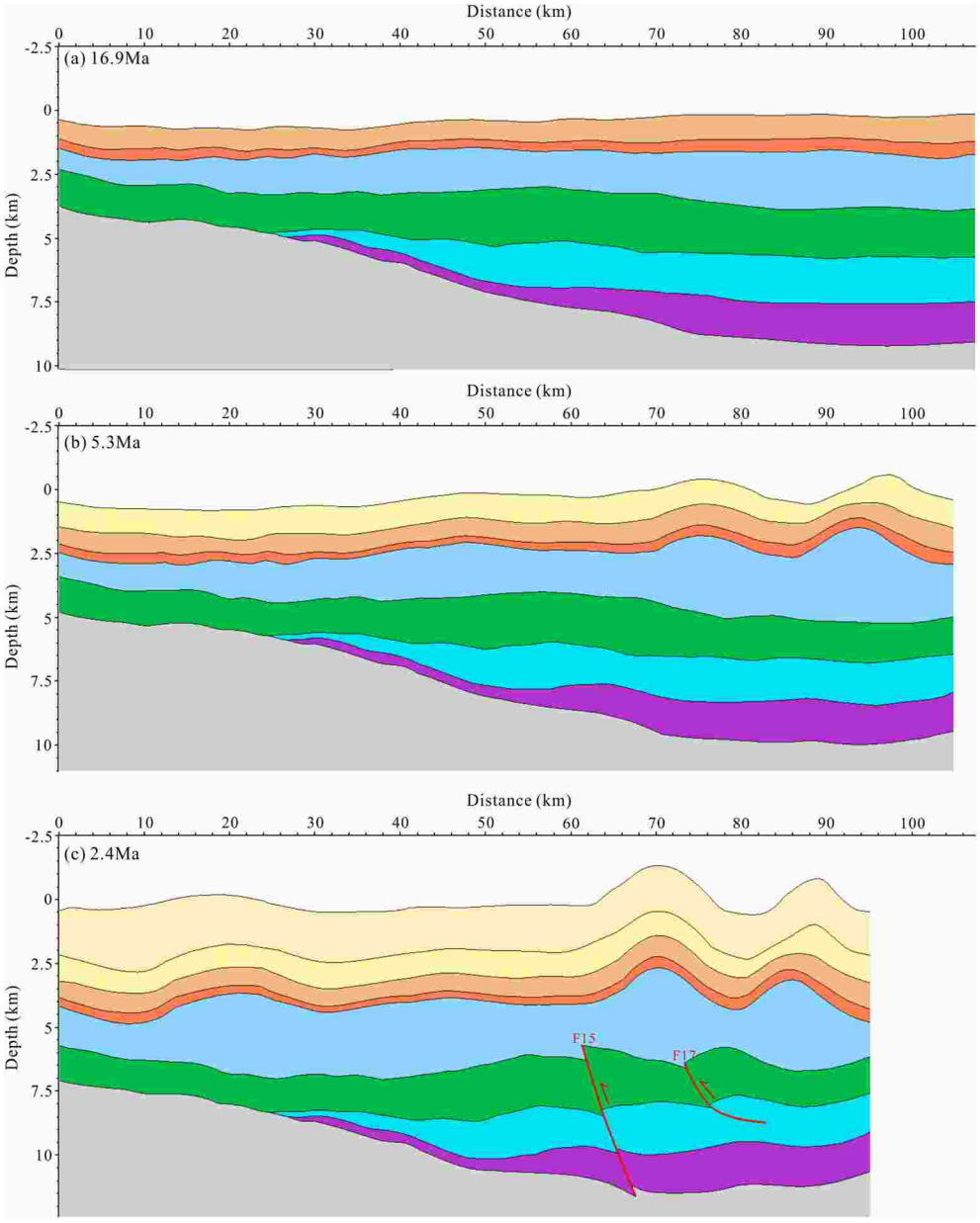

Fig. 5. Structural reconstruction of the seismic line (vertical exaggeration: 3 ×). Before the Jidike Formation deposition, the Kuqa Depression was at the extensional stage when all formations were normally deposited and therefore is not displayed here. After the Jidike Formation deposition (since 16.9 Ma), the Kuqa Depression was at the rejuvenated foreland basin stage. See text for details. Red line represents fault, named by red letters. See Fig. 4 for explanations of QA, BS, KA and BA. (For interpretation of the references to colour in this figure legend, the reader is referred to the Web version of this article.)

whereas the northern and southern parts experienced structural uplift and significant surface erosion related to increasing shortening, especially in the area to the north of the F15 fault. From 1.75 Ma to the present day (Fig. 5f), the stratigraphic and structural framework had only slight modification despite compressional shortening, and the Quaternary sediments were deposited in the accommodation space created between anticlines.

The results of structural restoration show a total shortening of about 35 km for the model since 16.9 Ma, accounting for 32.6% of the original section length before tectonic compression. This result is consistent with the concepts of Yin et al. (1998) and Allen et al. (1999), who assumed 20–40 km of crustal shortening in the Kuqa and surrounding areas obtained from balanced sections. It should be noted that the total shortening consists of thrust-faults sliding, folding, and rock bulk shortening directly related to porosity reduction (Burgreen-Chan et al., 2016). Although there is more than one scheme for structural reconstruction, the paleo-geometries in this study represents a geologically reasonable evolution process and can be used as a framework for basin and petroleum system modelling.

During structural reconstruction, some assumptions and simplifications have been made to reduce the complexity while respecting the regional structural evolution. For example, we assumed that at 1.75 Ma, the maximum erosion had been reached on the three anticlines and from 1.75 Ma to the present-day, only the Quaternary sediments were deposited without any erosion occurring, although there was a compressional shortening. In addition, it was considered that the thrust faults gradually occurred from north to south due to tectonic compression. However, the exact geologic time of faulting and the fault displacement at each time step is not well constrained. Furthermore, we also assume that during the tectonic uplift, sags sandwiched between the

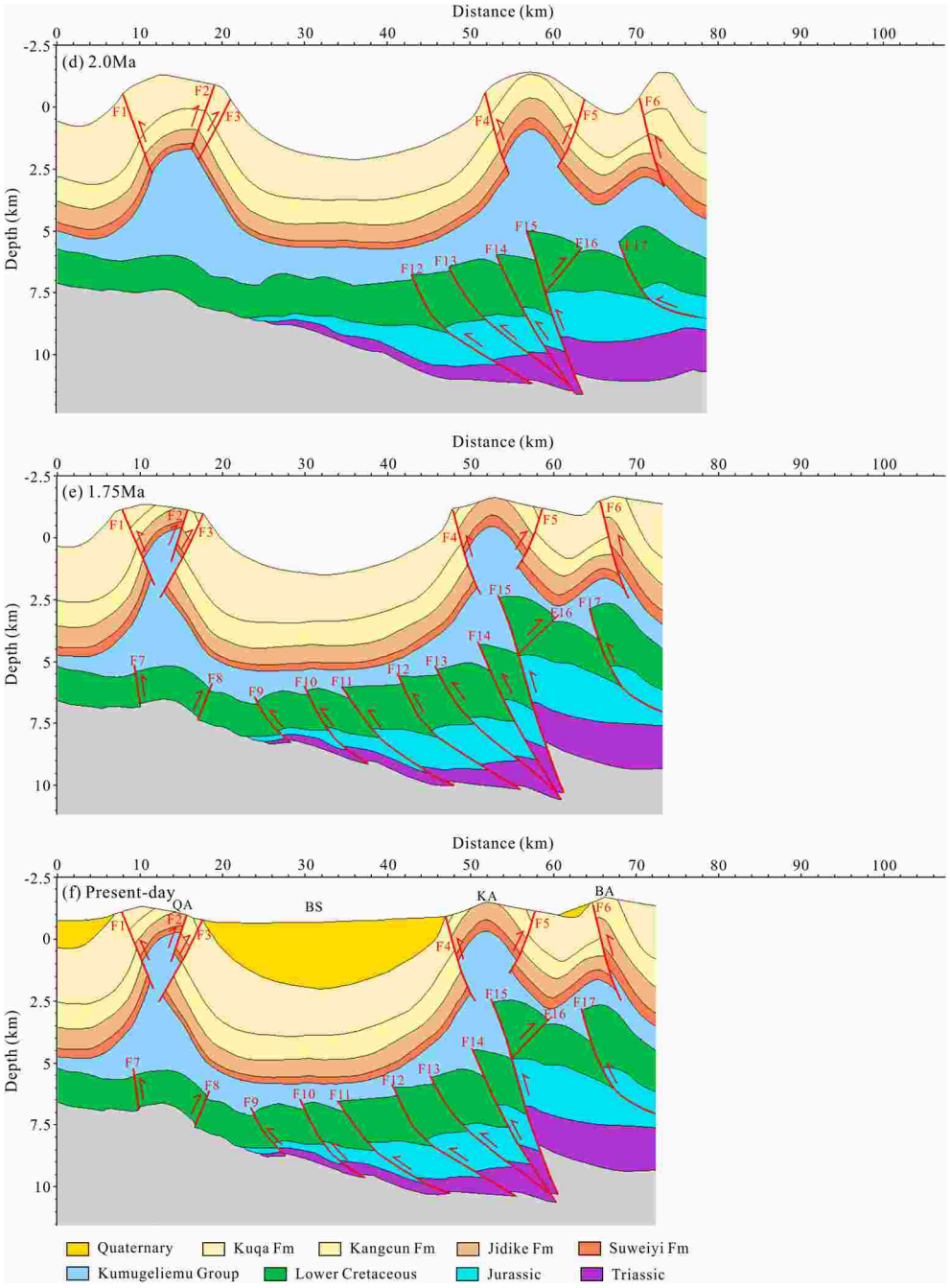

Fig. 5. (*continued*).

anticlines were not eroded, and the erosion restoration of anticlines is based on the thickness of the corresponding sedimentary stratum in the adjacent sags.

Finally, the restored geometries are input into a 2-D basin and petroleum system model to simulate pressure evolution using PetroMod. Mesozoic layers originally interpreted from seismic data were further refined to show more detailed pressure variations in the vertical direction (Fig. 6). Besides, the Kumugeliemu Group (Salt Group) also has been split into four members in BPSM according to lithologic variation. The thickness percentage of each newly-split formation refers to the wells penetrating the Mesozoic strata in northern and eastern Kuqa Depression and/or regionally average thickness from surface outcrops studies in the northern monoclinal belt (Wang et al., 2011; Li et al., 2012). It should also be noted that from a time step to the previous one during structural restoration, the newly-increased extension of the supra-salt section, dominated by fault-related fold deformation, is greater than that of the sub-salt section, dominated by thrust-imbricated structures. This results in a different length of the supra-salt section than the sub-salt section, which is not allowed in our simulator. To fluently perform basin and petroleum system modelling, the sub-salt section has been lengthened by compensating the layers to align its north (i.e., right) boundary with that of the supra-salt section.

4.2. Basin model

For the extensional stage (until 16.9 Ma) when the paleo-geometries were derived by the backstripping approach, compaction and pore pressure were obtained by iterative calculation based on initial porosity and the youngest thickness (i.e., 16.9 Ma). Ages of the deposition and erosion of formations control the calculation steps (Hantschel and

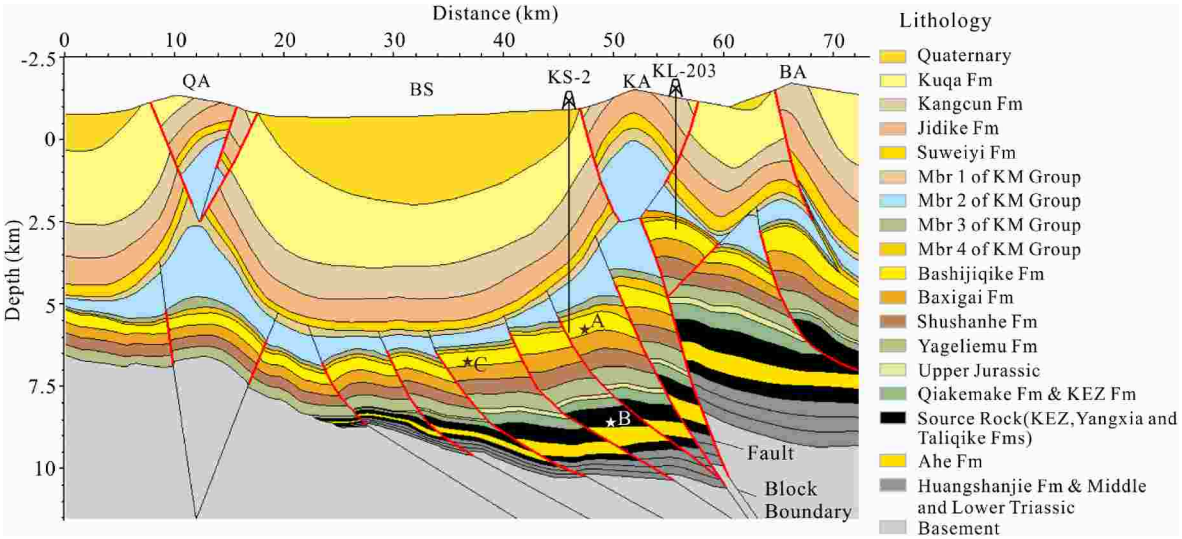

Fig. 6. Distribution of subdivided layers and the corresponding formation names in the 2-D geological model. See Table 1 for lithology of each subdivided layer, and the consistent lithology is prescribed for an entire layer. Block boundaries (black line) partially coincide with faults (red line). The stars represent the time-extraction locations of cells A, B and C in Figs. 16 and 17. KM=Kumugeliemu; KEZ=Kezilenuer. See Fig. 4 for explanations of QA, BS, KA and BA. (For interpretation of the references to colour in this figure legend, the reader is referred to the Web version of this article.)

Kauerauf, 2009). For the rejuvenated foreland basin stage (from 16.9 Ma to present day) when the paleo-geometries were derived from the structural restoration and input into BPSM as the predefined parameters. Each given paleo-geometry was used to calculate pore pressure taking into account its duration and shape, staring with the oldest geometry (i.e., 16.9 Ma) and simulating forward in time. The number of paleo-geometries instead of the deposition and erosion events determines the time resolution of forward modelling. Because compaction calculation is not needed due to the predefined thickness, porosity reduction associated with increasing effective stress is decoupled with changes in thickness (Baur et al., 2009). In addition, a single horizon is duplicated on the depth-axis due to lateral rock movement, which is not allowed in the model-gridding. To avoid this problem, the model is subdivided into many "blocks" bounded by thrust faults and horizons, and each block represents a "submodel" without vertical duplication of the horizon. These blocks in a paleo model are connected in terms of geochemical and geophysical properties during simulation; then, the calculated results can be transmitted to the corresponding block in the next model by the introduction of the so-called parent-child blocks concept (Hantschel and Kauerauf, 2009; Baur et al., 2009).

The Terzaghi model commonly used in traditional basin modelling assumes that the lithostatic pressure is equal to overburden loading and the horizontal effective stresses are a constant ratio (a parameter related to a specific lithology) of the vertical effective stress. Thus, any tectonic stress is neglected and the porosity reduction is only controlled by the vertical effective stress. This procedure also allows one-dimensional modelling of compaction, e.g., for one deep well (Terzaghi, 1943; Wang, 2000). Due to the reasons stated above, a Terzaghi based model is not suitable for reconstructing pore pressures and compaction in strongly deformed orogenic belts such as the Kuqa Depression. Instead, a poroelastic model needs to be applied as a real three-dimension model prescribed in this study. It could consider the relationship between the total stress, the pore pressure, and the total strain, in which two basic poroelastic behaviors, the solid-to-fluid and fluid-to-solid coupling, occur (Wang, 2000). The stress and strain herein are both bulk values, which means that this method can consider the impact of three-dimensional stresses on compaction, not only the vertical stress. Consequently, compaction is calculated by the mean effective stress rather than the vertical effective stress. The limitation of this poroelastic model is that rock failure and overpressure due to shear stress cannot be modelled (Hantschel et al., 2012).

4.2.1. *Lithologies*

Table 1 and Fig. 7 show the modelled lithologies and their corresponding petrophysical properties. The modelled lithologies were customized by mixing different components, which were then assigned to the corresponding layers in the model (Fig. 6). The mixing ratios are derived from the cuttings data of wells passing through and/or close to the seismic line. For example, lithologies of the Bashijiqike Formation and overlying strata are obtained from the wells located in the Kelasu structural belt. In contrast, lithologies of underlying strata, which are not penetrated by the wells in the Kelasu structural belt due to larger burial depth, are obtained from the wells (such as the KB-1 and HY-1) and outcrops located in the northern monoclinal belt, where the Mesozoic strata have less buried depth due to the intense uplift and erosion. Lateral variation of lithology for each layer is not considered due to the limited data.

The petrophysical properties of the mixed lithologies were first calculated from the mean values of the mixed components, taking into account the ratio of the mixed components, and were then calibrated with well data. Therefore, it is necessary to obtain the properties of each single component. The properties of components, such as the initial porosity, Poisson's ratio, density, and thermal conductivity were derived from a comprehensive literature review (Wang et al., 2005; Hantschel and Kauerauf, 2009; Zeng et al., 2010). Porosity-effective stress relationships of lithological components were based on Athy's compaction law (Athy, 1930); permeability-porosity relationships of lithological components were based on the multipoint model with values based on a comprehensive literature review by Hantschel and Kauerauf (2009). Different mean methods were selected, depending on the types of the physical quantities. The properties, such as porosity, Poisson's ratio, and density are classified as extensive parameters and were thus mixed using the weighted arithmetic mean; thermal conductivity and permeability are transport parameters and were mixed using the geometric mean.

After the petrophysical properties of the modelled lithologies were mixed using their respective mean methods, they were also calibrated with well data (Fig. 8). For example, porosity-effective stress relationships were calibrated with the converted porosities from sonic logs; permeability-porosity relationships were calibrated with both measured pressures and mud weight data; thermal conductivity was calibrated with measured temperatures including drill stem test (DST) and bottom-hole temperature (BHT). DST provides the most reliable temperatures which, however, are rare; even though BHT are generally lower than

Table 1
Rock properties of lithological mixtures assigned in this model[a].

Layer	Litho Mixture ratio (%)	Initial porosity (%)	Poisson's Ratio	Density (kg/m^3)	Thermal Conductivity (W/m/K)		Bulk Modulus (MPa)
					At 20 °C	At 100 °C	
Quaternary	30 cg, 35ss, 35sh	47.8	0.23	2707	2.47	2.30	From Compaction Curve
Kuqa Formation	10 cg, 55ss, 35sh	50.0	0.22	2711	2.75	2.51	
Kangcun Formation	8 cg, 50ss, 42sh	52.3	0.23	2710	2.61	2.41	
Jidike Formation	20ss, 20sil, 60sh	61.2	0.24	2708	2.04	1.99	
Suweiyi Formation	15ss, 20sil, 65sh	62.6	0.24	2707	1.96	1.93	
Mbr 1 of KM Group	60 sil, 40sh	61.0	0.25	2712	1.87	1.86	
Mbr 2 of KM Group	30sil, 40sh, 30sa	44.8	0.32	2592	3.85	3.31	
Mbr 3 of KM Group	40ss, 10sil, 50sh	56.9	0.23	2710	2.38	2.24	
Mbr 4 of KM Group	20 cg, 70ss, 10sil	40.2	0.2	2716	3.32	2.92	
Bashijiqike Formation	85ss, 15 sil	41.0	0.20	2720	3.54	3.10	
Baxigai Formation	85ss, 10sil, 5sh	43.8	0.21	2719	3.54	3.08	
Shushanhe Formation	80ss, 10sil 10sh	45.3	0.21	2718	3.39	2.97	
Yageliemu Formation	90ss, 10sil	42.4	0.20	2720	3.7	3.2	
Upper Jurassic	20ss, 50 sil, 30sh	56.7	0.21	2714	2.19	2.09	
Qiakemake & KEZ Formations	40ss, 30sil, 30sh	53.9	0.23	2714	2.49	2.32	
Source rock	85sh, 12 sil, 3co with 2.78% TOC and 373 mg/gTOC HI	70	0.24	2600	1.25	1.41	
Ahe Formation	10 cg, 80ss, 10sh	42.8	0.21	2696	3.23	2.86	
Huangshanjie Formation & Moddle and Lower Triassic	30ss, 20sil, 50sh	58.3	0.22	2710	2.23	2.13	
Basement	100 Schist	1.0	0.35	2740	2.90	2.62	

[a] The mixing ratios are obtained from cuttings data of the wells through and around the modelled section. All rock properties in the table were first calculated from the mean values of the mixed components considering the mixing ratio and then modified to achieve a good match between the modelled values and well data as shown in Fig. 8. Cg = conglomerate; ss = sandstone; sil = siltstone; sh = shale; sa = salt; co = coal; KM=Kumugeliemu; KEZ=Kezilenuer. The bulk modulus is calculated from the Terzaghi compressibility.

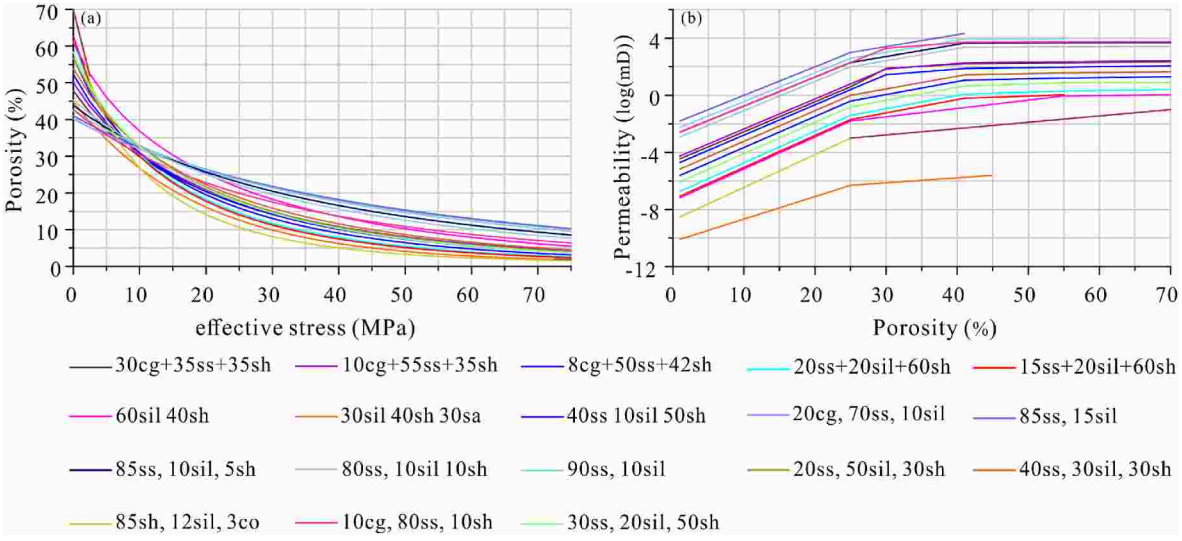

Fig. 7. (a) Porosity versus effective stress plots based on Athy's compaction law for modelled lithologies. (b) Permeability versus porosity plots based on the multipoint model (Hantschel and Kauerauf, 2009) for modelled lithologies. See Table 1 for explanations of lithological component abbreviations. Porosity-effective stress relationships and permeability-porosity relationships were based on the mean properties of lithological mixtures and then calibrated with well data in Fig. 8.

true formation temperature by an amount of up to ~10–15 °C, they are the most widely available temperature data and usually used as a rough estimate for temperature calibration in basin modelling (Peters and Nelson, 2012).

4.2.2. Faults properties

The fault geometries through geologic time, obtained from seismic interpretation and structural restoration, were given as a predefined input into the 2D model based on the finite element method, where faults were represented by the locally refined grid cells they passed through. Because fault width is usually in the range of several meters and much smaller than the grid cell of a basin scale model, the locally refined grid cells were applied, which was achieved by using irregular gridline spacing with higher gridline density near faults. The variable properties of faults over time were assigned to the fault cells.

Prior to 1.75 Ma, all faults were treated as active with significant displacement as shown in structural restoration and thus were set open to allow fluid flow along and across them. This was also suggested by previous studies, in which the migration of hydrocarbons along faults from deeper source rocks to Cretaceous reservoirs during the thermally-mature period was indicated (Jia and Li, 2008; Guo et al., 2016a). Open faults provided high permeability conduits, and structural duplication

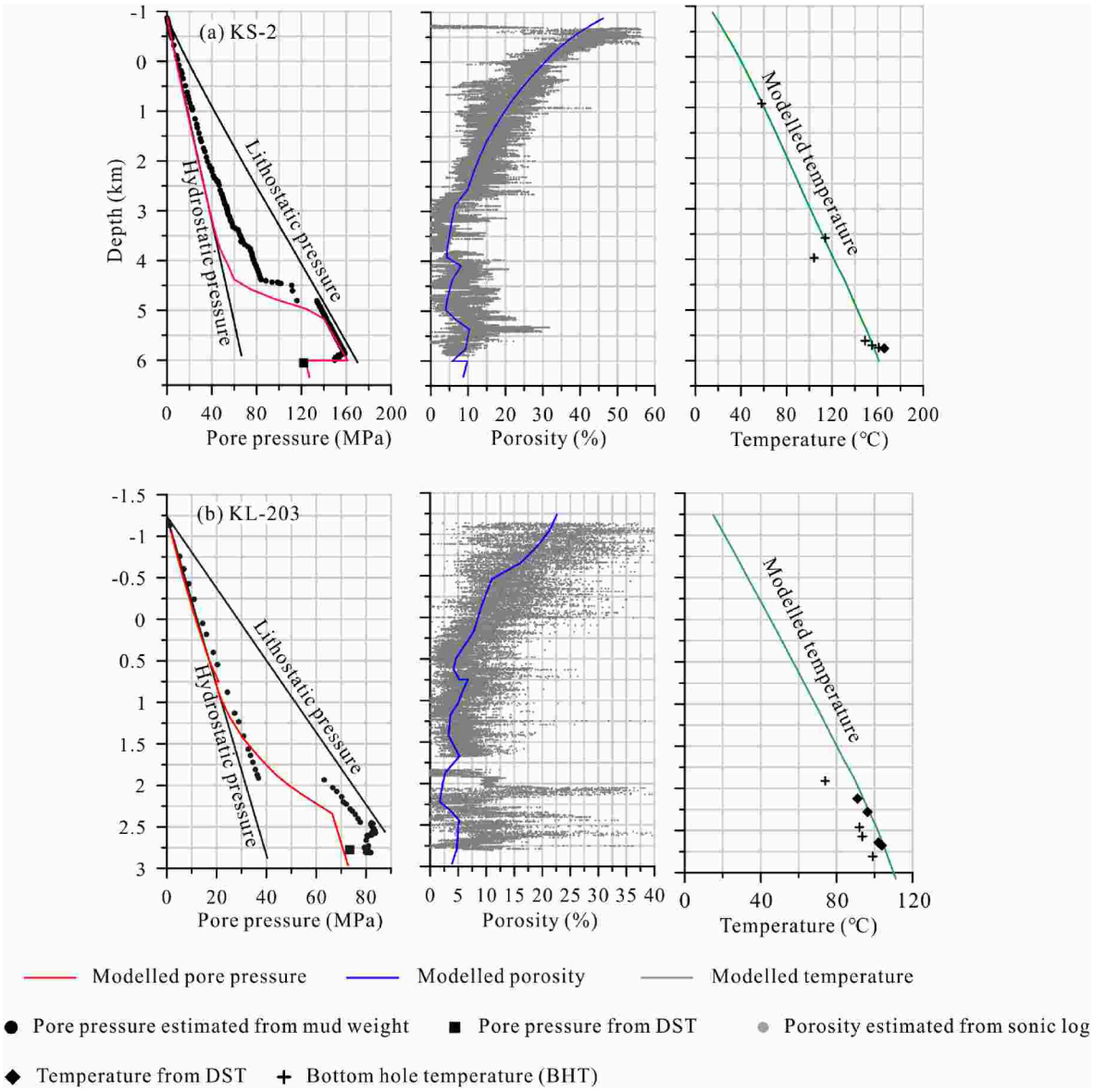

Fig. 8. Fit of modelled pressures, porosities and temperatures against measured values from wells KS-2 (a) and KL-203 (b), which were used to calibrate the petrophysical properties in Table 1 and Fig. 7. The good fit demonstrates that a good calibration has been achieved and the modelling results are reliable or at least not in conflict with well data. Pore pressures and temperatures from DST are the most reliable data and provide true formation properties. Mud weight and BHT are widely available data and are usually used as a rough estimate for pore pressures and temperatures in formation, respectively. See Figs. 1 and 6 for locations of KS-2 and KL-203.

due to thrusting (fault displacement) resulted in a significant burial increment for fault footwall and thereby increased pressures. Structural duplication has the same effect as rapid burial by sedimentation.

From 1.75 Ma to the present day, the structural restoration shows that the activity of faults ceased and they were thus set closed except for few newly-formed faults. Closed faults are also indicated by fault-related hydrocarbon traps (Fu et al., 2015; Guo et al., 2016c) and pressure contrasts on both sides of a thrust fault in our study area (Zhou, 2001; Fu et al., 2015). Closed faults can separate strata into several independent pressure systems, where fluid flow across a closed fault does not take place.

4.2.3. Boundary conditions and migration methods

The boundary conditions in basin modelling include thermal, pressure and displacement conditions. An average surface temperature history is assigned based on the global mean paleotemperature map after Wygrala (1989). Thermal history studies suggest that the Tarim Basin experienced a decreasing heat flow from the Mesozoic to the Cenozoic (Qiu et al., 2012). Therefore, in this model, a heat flow of 50–55 mW/m^2 during the Mesozoic and 40–50 mW/m^2 during the Cenozoic time is assigned (Li et al., 2010; Tang et al., 2014).

Like the thermal boundary conditions, the pressure boundary conditions also need to be predefined through the entire simulated geologic history in pressure forward modelling, including the upper, lower and side boundaries. The term upper-pressure boundary in basin modelling refers to the groundwater surface, which is usually assumed to be identical to the sediment surface (i.e., the topographic surface; Hantschel and Kauerauf, 2009). The types of upper-pressure boundary conditions are different between areas above and below sea level. The hydrostatic zero level, which refers to the constant reference level for the hydrostatic pressure calculation, can be artificially defined, since only pressure gradients rather than absolute values of pressures control water flow (Hantschel and Kauerauf, 2009). In the case of areas with relatively flat sediment surface or over a small scale, the sediment

surface can be treated as the hydrostatic zero level, and the pore pressure near the sediment surface is thus equal to the hydrostatic pressure. However, for areas with rugged topography or over a basin scale (e.g., the study area), the sediment surface is not suitable as the hydrostatic zero level, since it varies greatly over basin scale especially for tectonically active areas. Instead, the sea level is often assumed to be the hydrostatic zero level (Hantschel and Kauerauf, 2009). The hydrostatic pressure is then equivalent to the weight of the water column measured from the sea level; it has a positive value below and a negative value above sea level (Fig. 9). Thus it can be seen that the hydrostatic pressure is a theoretical pressure instead of a measurable pressure, whereas the pore pressure is a measurable one measured from the sediment surface (the groundwater surface). Consequently, a difference between pore pressure and hydrostatic pressure is caused above the sea level, referred to as the groundwater potential. Therefore, the groundwater potential is synonymous with overpressure, which induces topographic driven flow near the sediment surface.

In our model, the sea level acts as the hydrostatic zero level due to the rugged topography over basin scale during the structural evolution. For areas above sea level during structural evolution (e.g., the steep anticline), the sediment surface has a negative hydrostatic pressure, zero pore pressure, which is resulting in overpressure. Therefore, the boundary condition is set to the corresponding overpressure equal to the groundwater potential. For areas at or below sea level during structural evolution (e.g., the sags), the pore pressure at the sediment surface is equal to the hydrostatic pressure, and therefore the corresponding upper boundary condition is zero overpressure. In addition, both sides of the model are considered open, which means fluids are allowed to freely flow into or out of the model across the lateral boundaries, while the model base is defined as closed.

Geomechanical boundary condition in this simulation refers to bulk shortening (Burgreen-Chan et al., 2016). It is important to state that bulk shortening is different from total shortening. Bulk shortening is directly caused by porosity reduction. Total shortening, e.g., 35 km shortening derived from structural restoration in the Kuqa Depression, encompasses bulk shortening and structural shortening, the latter accommodating shortening from fault sliding and folding (Burgreen-Chan et al., 2016). Typically, bulk shortening only accounts for a small part of the total shortening (Berthelon et al., 2021). This has also been supported by

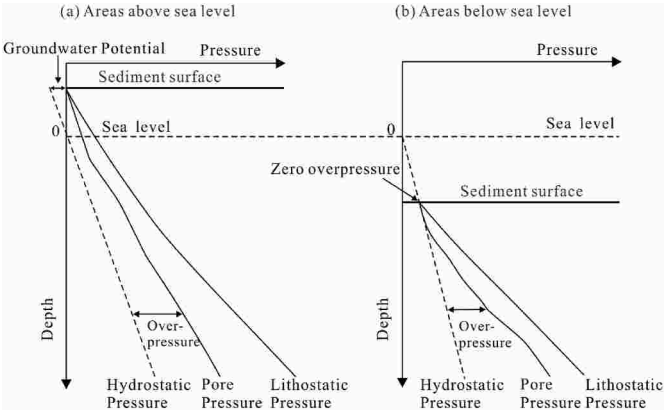

Fig. 9. Schematic diagram of the upper pressure boundary conditions for sediment surfaces of above (a) and below the sea level (b) in a region with rugged topography in basin model (modified after Hantschel and Kauerauf, 2009). The upper pressure boundary condition refers to the pressure state of the modelled sediment surface. The groundwater level is typically assumed to be identical to the sediment surface; the seal level acts as the hydrostatic zero level. Therefore, the hydrostatic pressure at the sediment surface above sea level has a negative value and the corresponding overpressure is set here; the hydrostatic pressure at the sediment surface below sea level is positive value to which pore pressure is equal, and zero overpressure is thus set at the upper boundary.

previous studies in the study area proving that compressional shortening in the South Tianshan area is mostly accommodated by thrust and fold structures (Yang et al., 2008). Considering that the various layers had undergone a certain degree of compaction before tectonic compression took place, bulk shortening may be only few percent of the section length in the Kuqa Depression. In this simulation, about 9 km of bulk shortening, accounting for about 12.5% of the present-day 72 km long section, is prescribed. This value is calibrated by pore pressure and porosity from KS-2 and KL-203 (Fig. 8) and is far less than the total shortening suggested by structural reconstruction.

The hybrid migration model used in this study was proposed by Hantschel et al. (2000) and is based on a combination of multi-phase Darcy flow and a buoyancy-based fluid migration, referred to as flowpath migration. A permeability threshold that distinguished between high- and low-permeability rocks and determines which method is used is set at 10^{-2} mD for 30% porosity in the model (Hantschel and Kauerauf, 2009). Rock permeability is controlled by porosity based on the relationship of permeability and porosity (Fig. 7b). In low-permeability strata, only Darcy migration approach is used to model flow of all pore fluids, in which the migration velocity is mainly controlled by the hydraulic pressure gradient (Baur et al., 2011). In high-permeability strata, different migration approaches are used, depending on the types of pore fluids. For example, Darcy approach is still used for pore water flow; however, for modelling of hydrocarbon flow the flowpath migration approach, in which buoyancy is the driving force for migration, is applied. Hydrocarbons move upwards within the high-permeability strata until they reach a seal and then move laterally along the tilted reservoir-seal interface.

4.3. Modelling results

In order to describe the spatial variations of overpressure on each section, blocks previously defined during model construction are applied in the following sections. The modelling results show that at 16.9 Ma, total overpressures are controlled by the burial depth. Overpressures mainly develop in the source rocks and its underlying strata, while the Cretaceous and the Cenozoic strata are normally pressured (Fig. 10a). Overpressures of 27.7 MPa–42.3 MPa develop in the Triassic system, generally greater than that in the Jurassic units. Lithology also affects the magnitude of overpressures. For example, the maximum overpressure within the Ahe Formation sandstones is 29.3 MPa, whereas up to 36.5 MPa in the Yangxia Formation dominated by shales (Fig. 10a). Overpressures in each layer decrease southward as the less burial depth. Overall distribution of pressure descripted above suggests that overpressure at 16.9 Ma is caused by disequilibrium compaction because overpressure primarily occur within and below low-permeability rocks with a large depth of burial.

At 5.3 Ma, the Bashijiqike Anticline and Kasangtuokai Anticline began to develop due to tectonic compression (Fig. 10b). For these two anticlines, the sediment surface is above the sea level, where zero pore pressure and the negative hydrostatic pressure are present (see previous boundary conditions for explanations), thereby inducing overpressure (Fig. 11). Herein, the negative hydrostatic pressure is equivalent to the weight of water column measured from the sea level. The pore pressure variation with depth follows a gradient of less than the hydrostatic pressure gradient, which is caused by topographic driven flow. Consequently, the overpressure gradually decreases with depth until the pore pressure is equal to the hydrostatic pressure, which also indicates that the effect of groundwater on overpressure is weakened with burial. In addition, the deposition of the Kangcun Formation and structural thickening increase overpressure in the Jurassic and Triassic sequences increased by about 3–4 MPa, but the Cretaceous rocks still maintained hydrostatic level.

At 2.4 Ma, the faults F15 and F17 formed in the Mesozoic strata; they were assumed to be open during the main activity phase. Pressure release occurs along open faults, which varies with formation

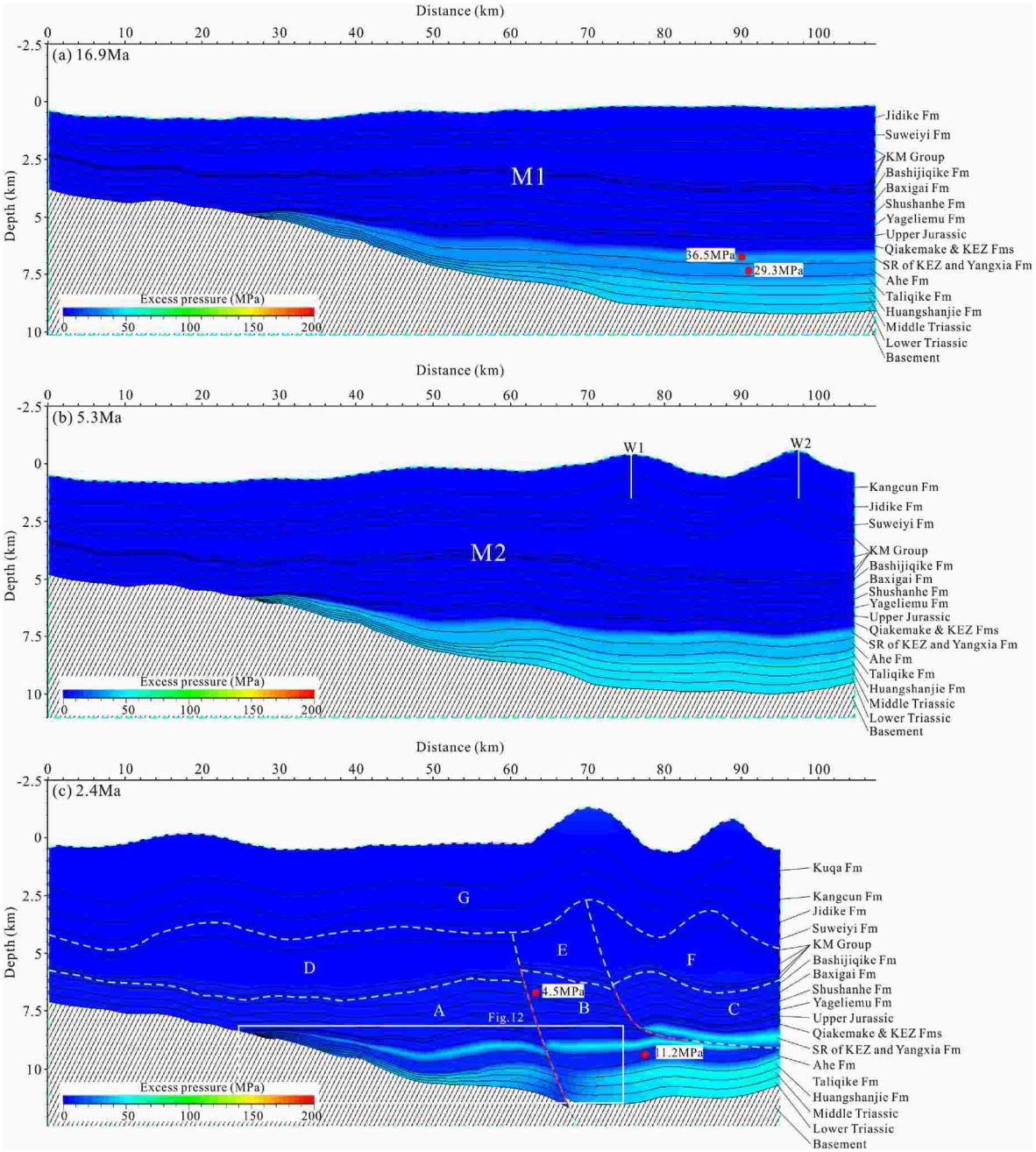

Fig. 10. Modelled overpressure evolution since 16.9 Ma. Cyan dashed lines represent block boundaries and red solid lines represent faults (see Fig. 5 for fault names). The block boundaries are usually composed of faults and horizons, although there are local cases where the block boundary cuts through the layers. The Kumugeliemu Group (Salt Group) is divided into some blocks separately because of its high ductile deformation characteristics. For the convenience of overpressure description, all blocks are named after a combination of letters and numbers in each time step. The pseudo wells from W1 to W6 indicate locations of 1-D extractions in Figs. 11, 13, 18 and 19, respectively. The open rectangles in (c), (d) and (e) indicate extraction locations of mini sections in Figs. 12 and 14, respectively. KM=Kumugeliemu; KEZ=Kezilenuer; SR=Source rock. (For interpretation of the references to colour in this figure legend, the reader is referred to the Web version of this article.)

permeability (Fig. 12). For the low-permeability Triassic and Jurassic source rocks, pressure-releasing influence is the greatest near the fault and gradually decreases away from the fault within a layer. However, for the permeable Ahe Formation, open faults affect the pressure distribution of the entire layer in which overpressure is uniformly decreased to about 11 MPa. This is caused by the formation's high hydraulic conductivity, enabling high lateral water-flow rates and the balancing of pressure throughout the layer. As a result, the overpressure within the Ahe Formation is 24.6 MPa lower than before the faulting occurred (i.e., 5.3 Ma), representing a significant decrease from the previous time step. Note that even though the rapid decrease in overpressure of the Ahe Formation promotes the fluid and pressure transmission from the adjacent low-permeability formations, which may temporarily increase pore pressure slightly in the Ahe Formation, the transmitted pressure is quickly readjusted due to the high hydraulic conductivity and open fault (Fig. 12). In this way, a hydraulically continuous transmission from the adjacent strata to the Ahe Formation to the open fault is maintained for a long geologic time due to the open

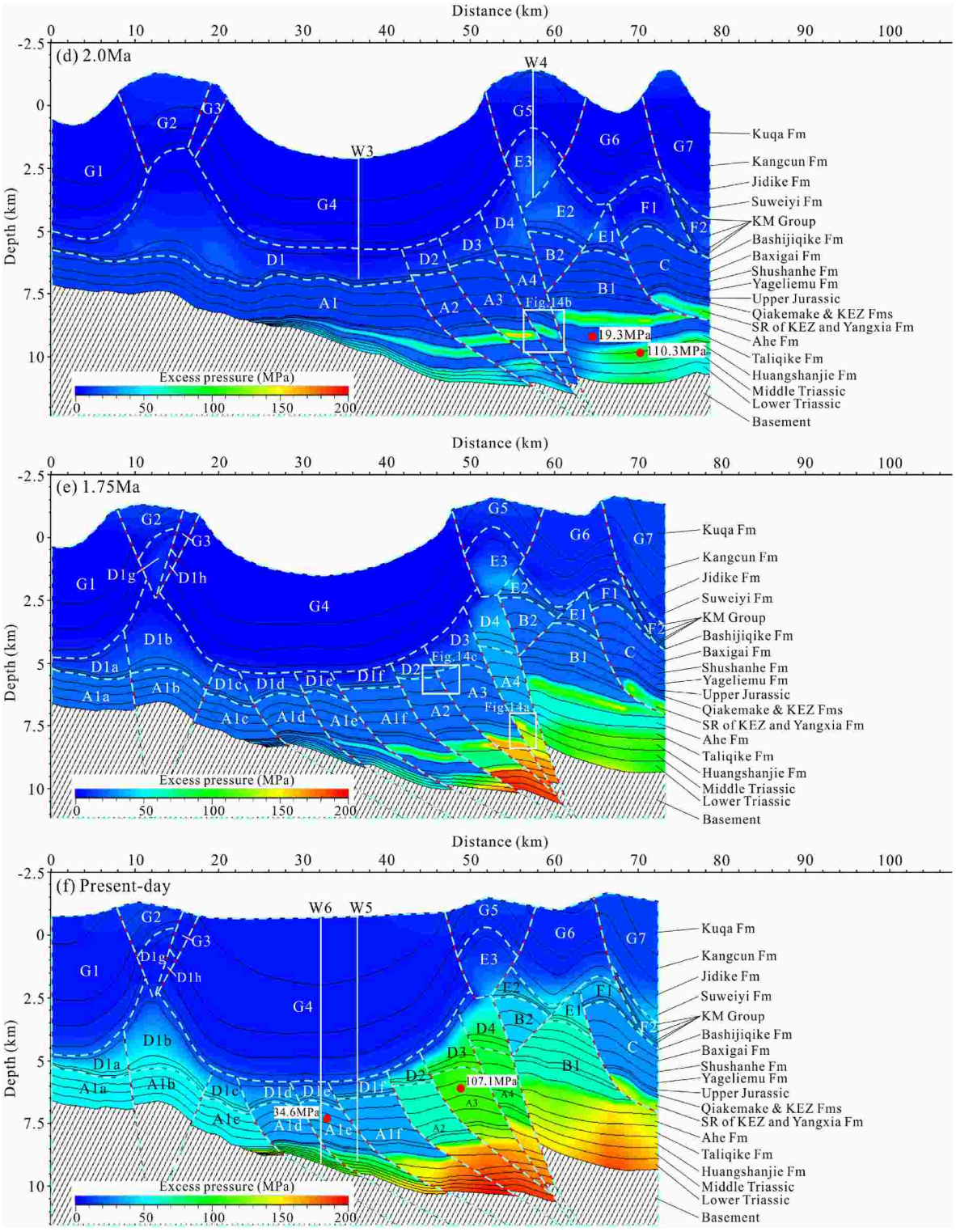

Fig. 10. (*continued*).

fault and the permeability difference between the Ahe formation and the adjacent strata. Relative to the permeable Ahe Formation, the transmission has less impact on the adjacent low-permeability formations because of the poor hydraulic conductivity, where overpressure first decreases within a narrow interval along the interface with the Ahe Formation, and a relatively great overpressure gradient within the low-permeability formations is thus generated as shown by the dense overpressure contours parallel to the interface (Fig. 12). In addition, Fig. 10c shows that overpressure begins to develop in the sequences above the source rock layer at 2.4 Ma, in which a uniform overpressure of 4.5 MPa appears in the interval from the Qiakemake Formation through the Bashijiqike Formation, and overpressure in the Kumugeliemu Group (Salt Group) remains in the range of 0–4.5 MPa.

At 2.0 Ma, continuous tectonic movement contributed to more thrust faults, more intense rock deformation and overpressures. Overall, Block B1 experiences a significant increase in overpressure due to tectonic

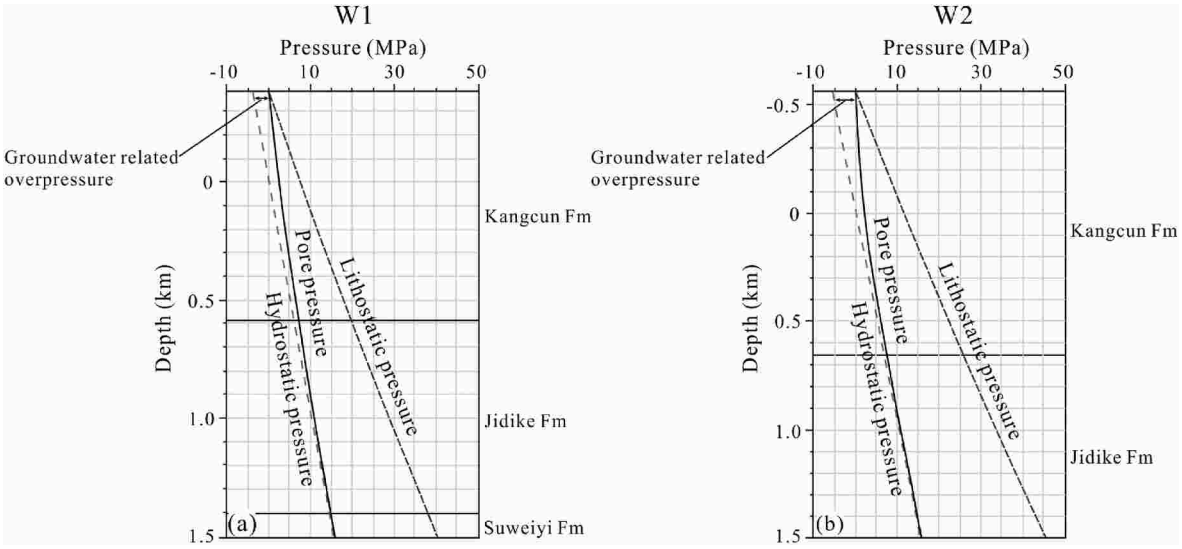

Fig. 11. 1D–extractions of pore pressures on Kasangtuokai anticline (a, W1) and Bashijiqike anticline (b, W2) at 5.3 Ma. The groundwater surface and hydrostatic zero level are assumed to match the topographic surface and sea level, respectively. Therefore, there is a difference between the pore pressure and hydrostatic pressure at the topographic surface, i.e., overpressure generation. The overpressure gradually decreases downward due to topographic driven flow. See Fig. 10b for extraction locations.

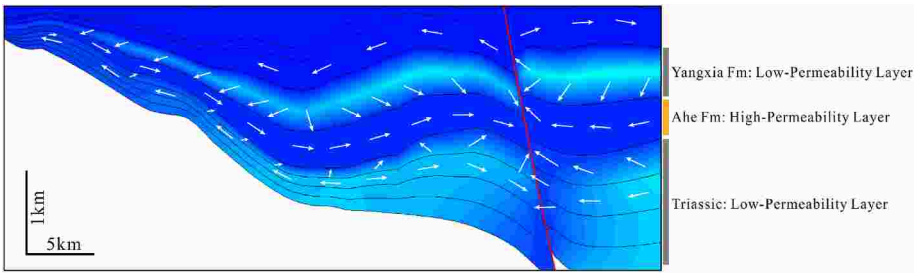

Fig. 12. The mini section shows the releasing effect of an open fault on overpressure at 2.4 Ma. Pressure release in permeable Ahe Formation is greater than that in the adjacent low-permeability layers, and pressure readjustment occurring in permeable layer also affects the overpressure distribution of the adjacent low-permeability layers. The white arrows indicate water-flow vectors. See Fig. 10c for location of the mini section.

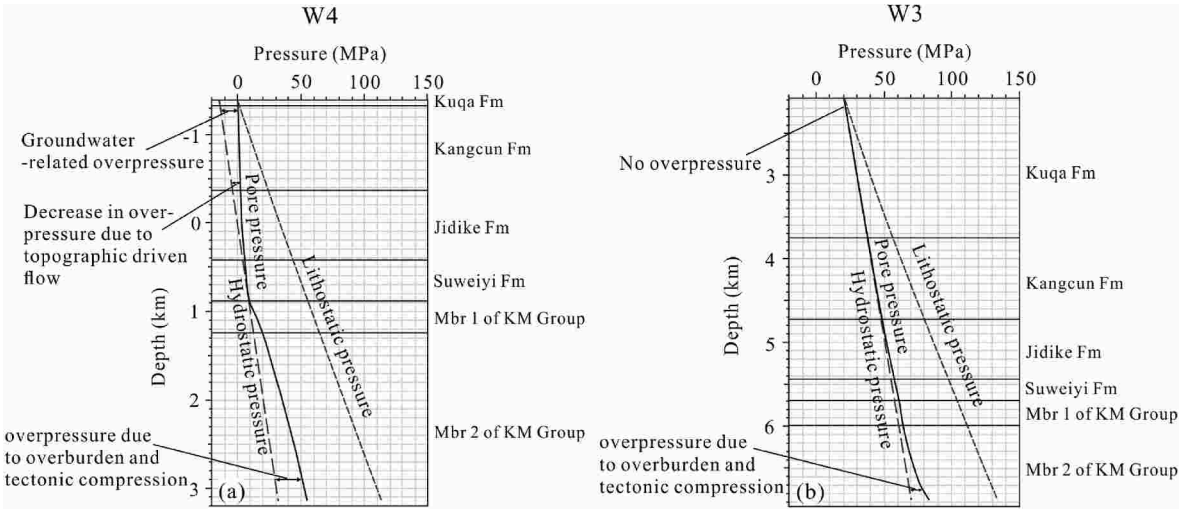

Fig. 13. 1-D extractions of pressures on the Kasangtuokai anticline (a, W4) and Baicheng sag (b, W3) at 2.0 Ma. Pore pressures vary with depth, affected by groundwater potential, topographic driven flow, and vertical loading and horizontal stress. KM=Kumugeliemu. See Fig. 10d for extraction locations.

compaction relative to the previous time step, despite the tectonic uplift associated with thrusting lowers its burial depth (Fig. 10d). The pressures difference between low- and high-permeability formations is further expanded, such as the overpressure of up to110 MPa in the Triassic strata and only 19 MPa in the Ahe Formation. Different degrees of dissipation of overpressure caused by open faults can still be observed

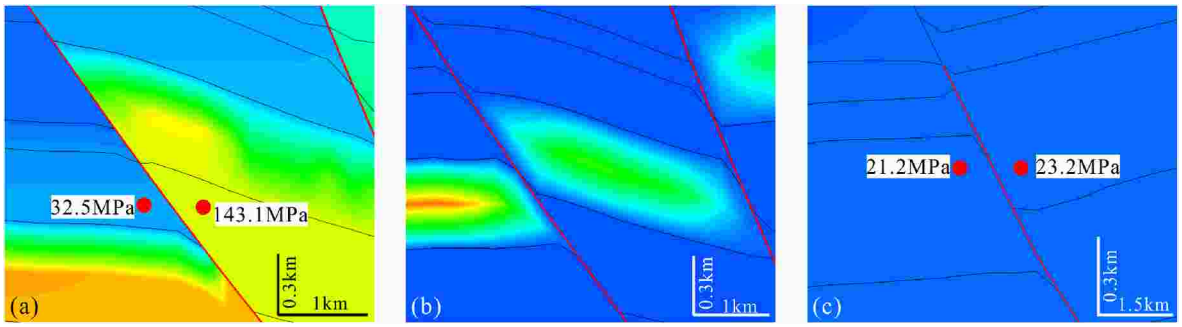

Fig. 14. (a) Shows sharply different overpressures in the Jurassic sequences on both sides of a closed fault at 1.75 Ma; (b) shows a gradual change in overpressure across open fault at 2.0 Ma; (c) shows that difference of overpressure is quite small within the Cretaceous rocks on both sides of the closed fault at 1.75 Ma, because of their good hydraulic-connection in previous time step. See Fig. 10e for extraction location of a and c, and Fig. 10d for b.

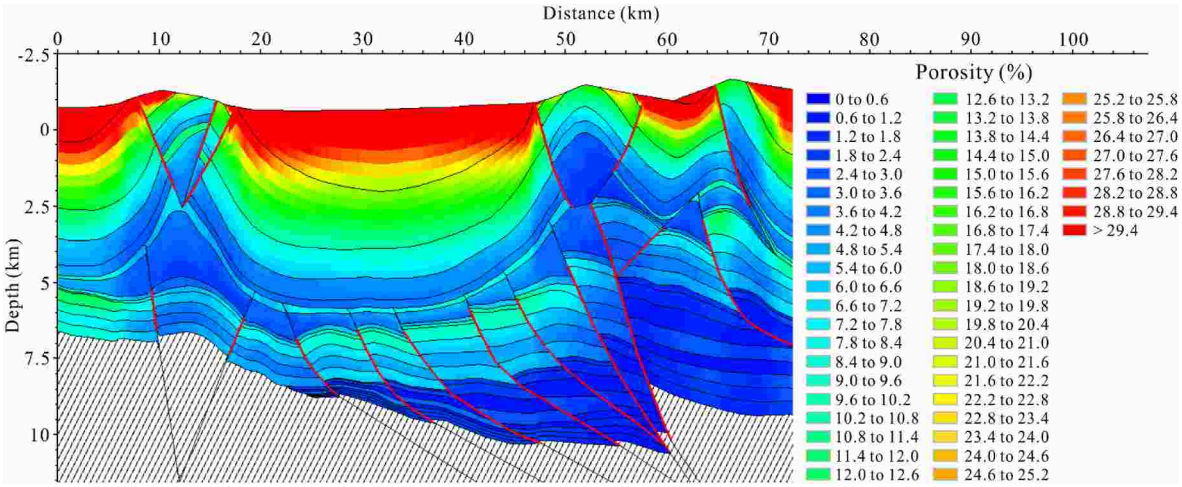

Fig. 15. Distribution of modelled porosity at present day. The present-day porosity map indicates the magnitude of rock compaction, which has a good match with overpressure distribution at present day.

in Blocks A1, A2, A3 and A4. The overpressure in the Lower Cretaceous is uniformly distributed through each layer due to good hydraulic connection. The geometries of the folds were further reinforced with tectonic compression, and the corresponding pressure vs. depth profiles are affected by a combination of groundwater potential, topographic driven flow, and mechanical loading. Pore pressure-depth relationships for anticline and syncline show different characteristics (Fig. 13). As mentioned previously, the sediment surface of the Kasangtuokai anticline is above the sea level, and the resulting groundwater potential shows an overpressure of 14.4 MPa at the sediment surface (Fig. 13a). At the same time, the overpressures within the Kuqa through Suweiyi Formations decrease downward, because the pore pressures increase with depth along a gradient of less than hydrostatic pressure gradient caused by the topographic driven flow; within the Kumugeliemu Group (Salt Group) overpressure begins to gradually increase due to vertical loading and horizontal stress. In contrast, the sediment surface of the Baicheng sag is below the sea level (Fig. 13b). The pore pressure at the sediment surface is equal to the hydrostatic pressure and increases within the Kuqa and Kangcun Formations along the hydrostatic pressure gradient until overpressure generation generates in the Jidike Formation.

At 1.75 Ma, the section experiences a significant increase in overpressure because of the strongest compression, even though tectonic uplift and erosion take place (Fig. 10e). In this section, the newly-formed faults (i.e., F7–F11) are considered open, allowing fluid-flow and pressure transmission across faults, while the faults F12–F17 are assumed to be closed considering that they had almost reached their maximum displacements at 1.75 Ma. As a result, the pressures of adjacent closed fault-bound compartments are sharply different, such as overpressure of only 32.5 MPa on the left side of the closed fault and up to 143.1 MPa on the right side (Fig. 14a), which is opposite to the transitional pressure distribution across the open fault at 2.0 Ma (Fig. 14b). The amount of overpressure difference between adjacent compartments depends not only on the fault sealing at 1.75 Ma, but the pore pressure history of compartments. For example, Fig. 14c shows that there is a quite limited overpressure difference for the Lower Cretaceous rocks on both sides of the closed fault, because they have good hydraulic lateral-connection related to fault opening at 2.0 Ma. Even though the anticlines experience varying degrees of denudation (denudation thickness ranging from 1300 m to 2000 m), increase in overpressures still occurs within these anticlines resulting from bulk shortening of rocks (Fig. 10e).

At the present day, overpressures in the cross-section vary greatly in both vertical and horizontal directions due to sealing of salt-bearing layer and fault compartmentalization (Fig. 10f). Vertically, overpressure of the Cenozoic units is much smaller than that of the Mesozoic, where it is extremely difficult for overpressure to be transmitted upward into the Cenozoic strata across the low-permeability seal layer. Laterally, the Mesozoic strata underlying anticlines are more overpressured than those beneath the sag, because rocks underlying anticlines experience more intensive compaction during tectonic compression. For example, the Lower Cretaceous rocks in Blocks A3 have overpressure of up to 107.1 MPa, while overpressure of only 34.6 MPa is built up in Block A1e beneath the sag. In fact, the present-day overpressure distribution has a good consistency with rock compaction (Fig. 15), which may indicate

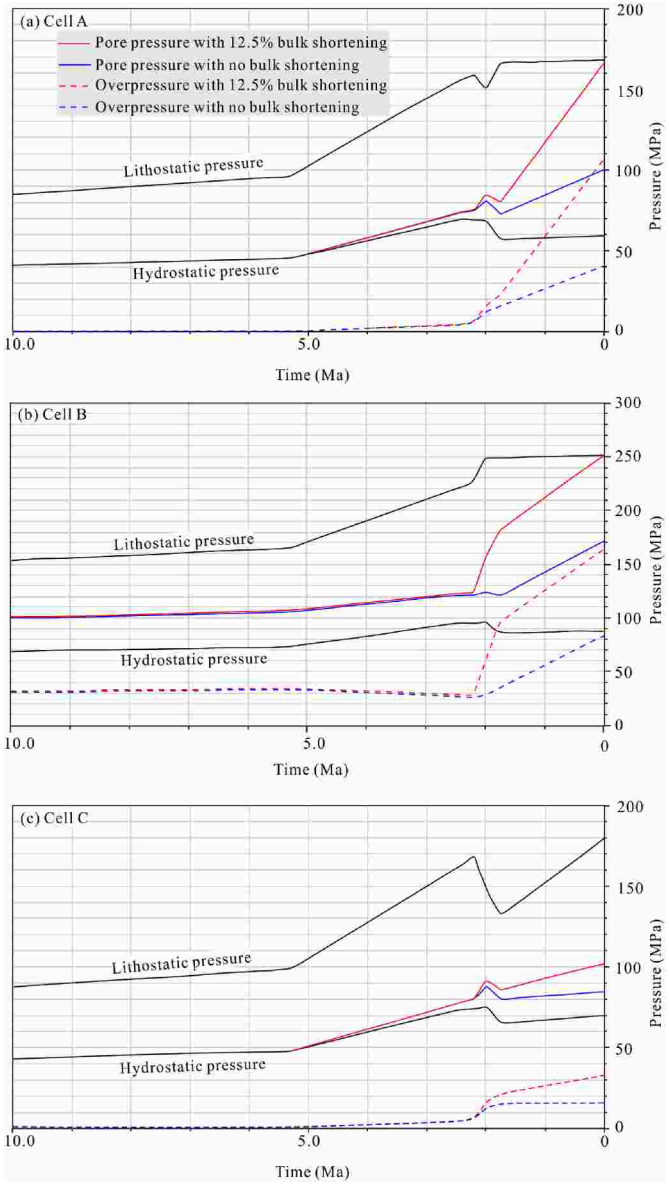

Fig. 16. Time extractions of pressure showing the contribution of tectonic compression to overpressures through geological time (extraction locations of (a), (b) and (c) corresponding to cell A, B and C in Fig. 6, respectively). Overpressure caused by the bulk shortening (the difference between blue and red lines) began at 2.4 Ma, and the contribution of tectonic compression varies with lithology and deformation (compaction) magnitude. (For interpretation of the references to colour in this figure legend, the reader is referred to the Web version of this article.)

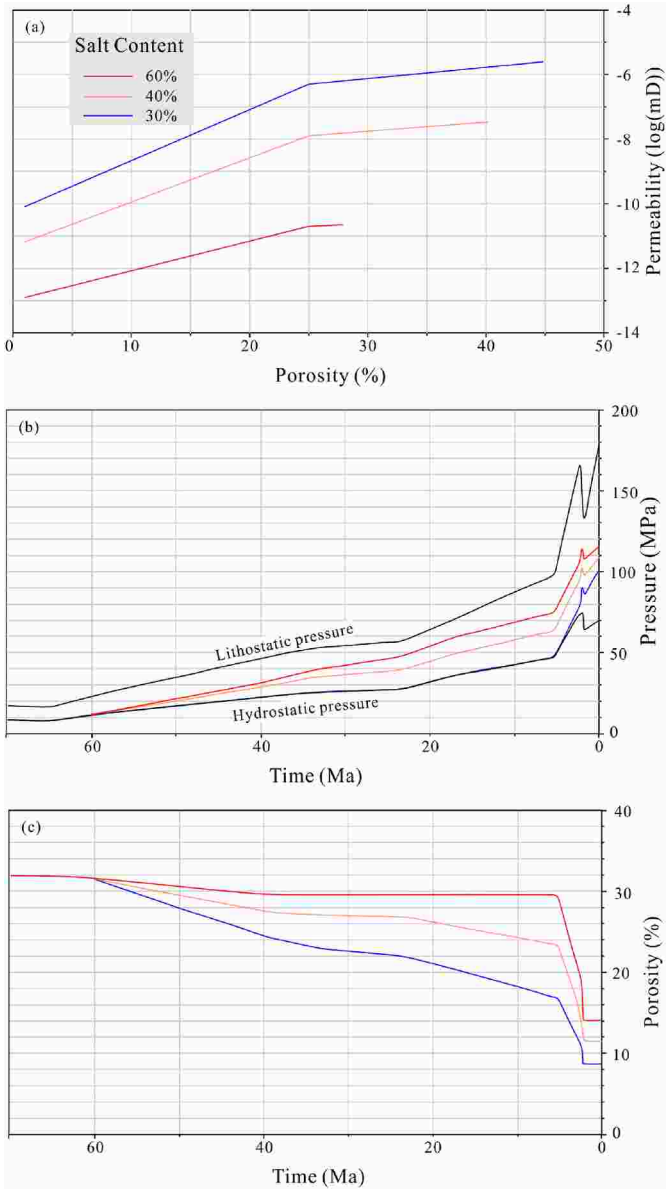

Fig. 17. Permeability-porosity relationships (a), evolution of pore pressure (b) and porosity (c) in cell C (see Fig. 6 for extraction location) for comparison of varying salt content of the seal layer. Permeability for each case is calculated from the geometric mean values of the mixed components, taking into account the ratio of the mixed components. Increasing salt promotes the onset time and magnitude of overpressure and delays rock compaction.

that mechanical compaction is the dominant cause of overpressure. Fig. 10f also shows that the overpressure contours located in lower parts of Blocks A1f, A2, A3, A4 and B1 have a good match with profiles of the corresponding overlying anticlines (Kasangtuokai anticline and Bashijiqike anticline). A combination of deeper burial and continuous horizontal-compression leads to the extremely low porosity and permeability, where fluids can hardly escape from pore spaces. Consequently, pore fluids sustain most of the additional overburden load resulted from anticline development. Additionally, our model suggests that overpressure development is also related to the structural and burial history, such as overpressure of block B2 is lower than that of adjacent blocks, because block B2 has experienced significant uplift along back-thrust faults since 2.0 Ma.

5. Discussion

5.1. The effect of tectonic compression on overpressure

To evaluate the effect of tectonic compression on pore pressure evolution in the study area, another scenario with no bulk shortening has been investigated in comparison with the base case scenario which has a 12.5% bulk shortening. The overpressure evolutions from the two scenarios show little difference before 2.4 Ma and significantly deviate after 2.4 Ma (Fig. 16). The overpressure magnitude (the difference between blue and red lines in Fig. 16) caused by bulk shortening depends on the lithology and compressional deformation. For example, in the Bashijiqike Formation sandstone in Block A3 beneath the anticline (Fig. 16a), from 2.0 Ma to present day overpressure due to the bulk shortening increases from 3.5 MPa to 66.4 MPa, accounting for

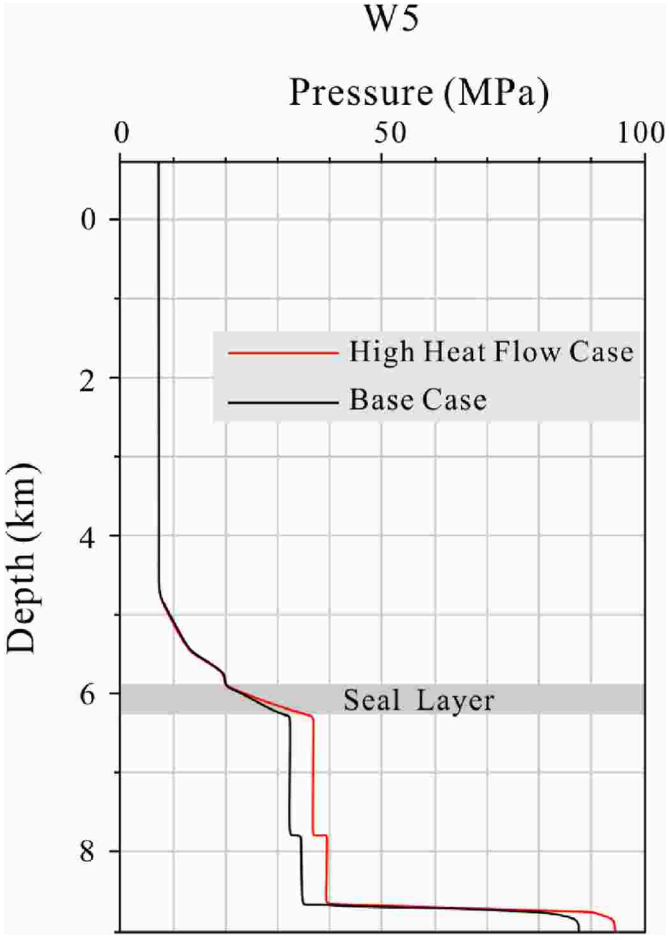

Fig. 18. 1-D extraction of overpressure in W5 showing the impact of increasing heat flow on pressure. The overpressure due to aquathermal expansion below the seal layer is greater than that above the seal layer. The black line represents the base case with 50–55 mW/m^2 during the Mesozoic and 40–50 mW/m^2 during the Cenozoic; the red line represents the high heat flow case with a time-constant value of 60 mW/m^2. See Fig. 10f for extraction location. (For interpretation of the references to colour in this figure legend, the reader is referred to the Web version of this article.)

22.3–61.9% of total overpressure with the 12.5% shortening scenario. For the Yangxia Formation shale in Block A2 (Fig. 16b) during the same time period, overpressure resulted from the bulk shortening ranges from 31.4 MPa to 80.3 MPa, accounting for 49.1–63.5% of total overpressure, which indicates that the impact of tectonic compression on pore pressure in shale is greater than that in the sandstone. However, for the Bashijiqike Formation sandstone in Block A1f beneath the sag (Fig. 16c), the magnitude of overpressure caused by bulk shortening is in the range of only 3.5–17.4 MPa from 2.0 Ma to present day, much smaller than that in Block A3. This is because the sag zone experienced a weaker deformation and smaller mean stress than the anticlines.

5.2. The effect of salt content on overpressure of the underlying strata

The salt content in the Member 2 of the Kumugeliemu Group (Salt Group) has a significant impact on the development and preservation of overpressure within the underlying strata. Previous works also suggested that overpressure distribution in the reservoir correlates with the thickness of the salt in the Kuqa Depression (Zhou, 2001; Jia and Li, 2008). Study on cuttings from 10 wells in the Kelasu structural belt shows that the salt content ranges from 16% to 62%. In this study, apart from the base case of 30% salt, two other scenarios with 40% and 60% salt content, respectively, were tested to examine the effect of salt on pressure development. As mentioned previously, permeability of the salt-bearing layer for each case was calculated from the geometric mean values of the mixed components, taking into account the ratio of the mixed components. The calculation results show that permeability decreases with the increase of salt in the formation (Fig. 17a). The pressure modelling shows that higher salt content leads to earlier onset time and greater magnitude of overpressures. For example, for the cell C extracted from the Bashijiqike Formation (Fig. 17b), the starting time and magnitude of the present-day overpressure for the 30% salt scenario is 5.3 Ma and 32.4 MPa, respectively, while the starting times for the scenarios of 40% and 60% salt are both 60.3 Ma, and the corresponding overpressures at present day are 40.6 MPa and 46.2 MPa, respectively. The modelled porosity also suggests that increasing salt retards the reduction of porosity during structural evolution. From 60 Ma to 5.3 Ma, the porosity of the cell C with 30%, 40%, and 60% salt decreases by 15%, 8% and 2%, respectively; the corresponding porosity at present day remains at 8.7%, 11.5%, and 14.1%, respectively (Fig. 17c).

5.3. Sensitivity analysis of heat flow

A scenario has been run to determine the influence of aquathermal pressuring, where a higher and time-constant heat flow of 60 mW/m^2 is used. Change in heat flow can affect pressures above and below the seal layer (Fig. 18). For example, higher heat flow increases overpressure at present day by about 4.3 MPa below the seal layer relative to the base case (i.e., the heat flow scenario of 50–55 mW/m^2 during the Mesozoic and 40–50 mW/m^2 during the Cenozoic used in the temperature boundary condition mentioned previously). However, for strata above the seal layer, characterized by higher permeability and poorer sealing efficiency, the higher heat flow scenario is almost indistinct from the base case scenario. This different changes in overpressure below and above the seal layer indicate that seal effectiveness may play an important role in aquathermal pressuring. Aquathermal pressuring was firstly proposed by Barker in 1972, who emphasized that a rise in temperature leads to pore-fluid expansion and resulting abnormally high pressure if a fluid system is characterized by a very good seal with low permeability (Barker, 1972). Therefore, the overall impact of aquathermal expansion on pore pressure depends on how well the pressure system becomes isolated, which explains the different changes in overpressure below and above the seal layer in our study area. The influence of aquathermal pressuring may be weakened by both 1) fluid leakage due to imperfect sealing and 2) reduced fluid-viscosity related to increasing temperature in the actual geological environment. In any case, the contribution of aquathermal pressuring on overpressure is much smaller compared to other pressuring factors (Luo and Vasseur, 1992, 1993; Swarbrick et al., 2002).

5.4. Overpressure related to gas generation

Hydrocarbon generation, especially gas generation, often leads to overpressures in sedimentary basins due to volume expansion of pore fluid (Swarbrick et al., 2002). The source rocks in the Middle and Lower Jurassic as well as the Upper Triassic have reached a high maturity in the Kuqa Depression (Qin et al., 2007). The Lower Cretaceous Bashijiqike Formation and sandstone units at the base of the Paleogene Kumugeliemu Group are the main gas-producing reservoirs in the area. To evaluate the impact of gas generation on pore pressure, we run two models with and without hydrocarbon generation, respectively. Considering the lithology, sedimentary environment, and geological age of the source rocks, a type III kinetic proposed by Ungerer (1990) for coaly source rocks was selected in the model. Physical and chemical concepts about the calculation of gas generated pore pressure have been described in detail in Hantschel and Kauerauf (2009). Modelled results show that the magnitude of overpressure caused by gas generation varies greatly between source rock and reservoir. In pseudo well W6 (Fig. 19), the overpressures in the Jurassic and Triassic source rocks

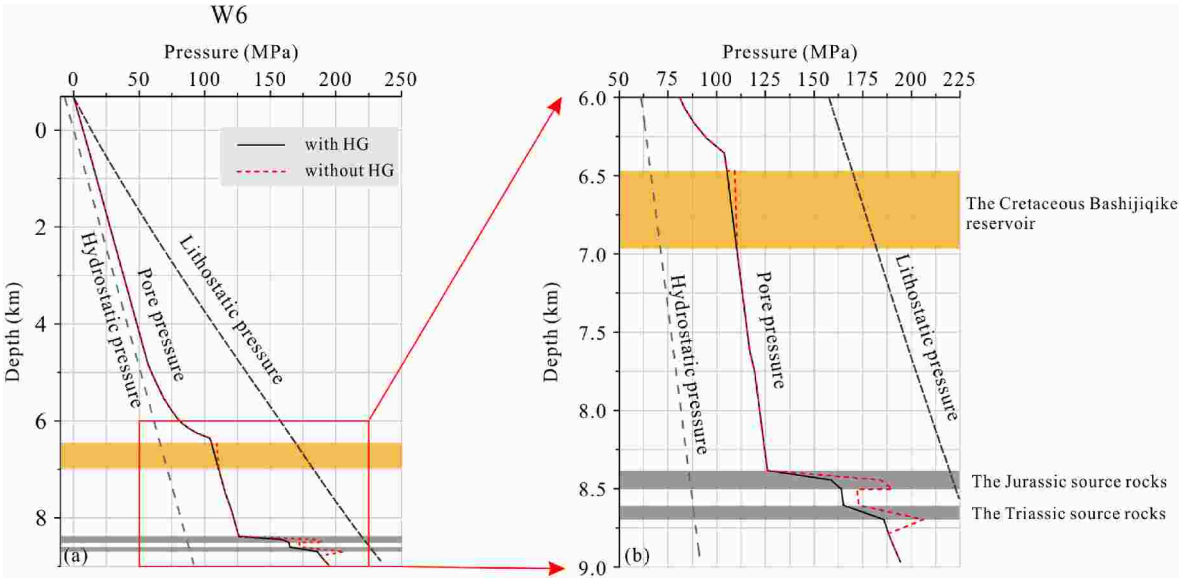

Fig. 19. 1-D extraction in W6 showing the additional effect of gas generation on overpressure. The magnitude of overpressure caused by gas generation in source rocks is significant, whereas it is quite weak in reservoir rocks. The discrepancies are mainly attributed to the differences in i) absolute permeability/retention and ii) hydrocarbon saturation and the resulting relative permeability. (b) Is the magnified area of the red box in (a), HG = hydrocarbon generation. See Fig. 10f for extraction location. (For interpretation of the references to colour in this figure legend, the reader is referred to the Web version of this article.)

resulting from gas generation reach 26 MPa and 20 MPa, respectively, while it is up to only 4 MPa in the in-situ Cretaceous reservoir, even though there is a relatively higher hydrocarbon saturation within the reservoir of the selected pseudo well than the surrounding ones. The discrepancies in the amount of overpressure generated by gas generation between source rock and reservoir can be explained by the following factors (Swarbrick et al., 2002): in source rocks where the hydrocarbon phase is typically dominant, a significant overpressure related to gas expansion is easily achieved in hydrocarbon-saturated pores; the presence of multiple phases fluids (water, oil and gas) greatly decreases the relative permeability, which promotes a high-magnitude overpressure generation. By contrast, reservoir rocks contain fluids dominated by water phase, leading to less volumetric expansion and higher relative permeability. In addition, migration within reservoirs redistributes overpressure related to gas generation throughout the connected pores, such that the pressuring effect in reservoir rocks is quite weak. Luo and Vasseur (1996) also suggested based on a numerical model that the pressuring effect of gas generation in source rocks is much greater than that in reservoir rocks.

5.5. Petroleum implication

The overpressure development under the salt-bearing seal layer has significant implication for petroleum exploration in the Kuqa Depression. The Bashijiqike Formation, as the dominant reservoir, is directly below the seal layer and experiences increasing overpressure since 2.4 Ma, when the Kuqa Depression has been at the stage of the strongest compression. The combination of overpressure and the effective seal layer can significantly retard the porosity loss and prevent petroleum leakage in the reservoir. This is especially important for reservoirs located in compressional basins. Many petroleum exploration activities have also suggested that strong overpressure, especially that related to the salt layer, increases the possibility of oil and gas entrapment. For example, large and medium-sized oil and gas fields discovered in the Kuqa Depression (Tang et al., 2004), the Gulf of Mexico, the South Atlantic Basin of offshore Brazil, West Africa, and North Sea (Akrout et al., 2016) have a close link with overpressure related to salt.

The evolution of fault properties through time has an important impact on the lateral migration of oil and gas within the source rock and the vertical migration from the source rock to the reservoir along the open faults. Opening of fault results in rapid dissipation of overpressure of rocks near the fault, thereby promoting a lateral flow toward the fault within the source rock due to the presence of overpressure gradient (Fig. 12). The poor hydraulic connection in the source rock layer can maintain this overpressure gradient for long time, which helps to form a constant convergence of the generated hydrocarbon toward the fault and subsequent vertical migration to the shallower reservoir along the open fault. When the fault is closed, it acts as part of the pressure compartment to help to preserve oil and gas. There have been many reports demonstrating this role of faults in hydrocarbon migration (O'Connor et al., 2008; Zhuo et al., 2014; Neumaier et al., 2014) and preservation (Allan, 1989; Mildren et al., 1994; Zhou, 2001; Underschultz and Strand, 2016) in the Kuqa Depression and other areas around the world.

5.6. Model limitations

There are usually significant uncertainties in the basin geometry for each time step and formation thickness input into the model, mainly due to the following two reasons: (1) The interpretation of horizons and faults from the seismic section is often uncertain due to poor local quality, especially for the sub-salt sequence, and (2) some simplifications were applied during the structural reconstruction process. For example, the effect of overpressure on porosity preservation was not considered, resulting in a larger thickness of the restored strata. The geometry restoration of the salt-bearing layer is very challenging because the kinetic behavior of salt-flow related to its highly ductile nature is difficult to model during structural restoration. In this study, the paleo-geometry of the salt-bearing layer at each time step is indirectly obtained by the structural restoration of supra- and sub-salt sequences. This is an acceptable procedure considering the plastic-flow behavior of salt. Besides, the viscous behavior would change stresses in salt during tectonic compression and locally redistribute mean stress within the salt-bearing layer, thereby affecting the pressure distribution. However, in the process of pressure simulation the viscous behavior is not calculated due to the software limitations. Instead, salt is only modelled as a regionally good seal associated with a very low permeability.

In addition, the timing of the fault activity and their displacements at each time step are poorly constrained, although the fault evolution in the structural reconstruction is generally consistent with the knowledge of the regional tectonic development. Because the TecLink approach in PetroMod uses reconstructed geometries as input parameters for the numerical basin model (Baur et al., 2009), the quality of basin and petroleum system modelling significantly depends on the reconstructed input geometries. In any case, the geometry has been treated as carefully as possible in order to create a consistent model.

Furthermore, the model does not account for plastic deformation of rocks, leading to extremely high rock stresses, where no rock failure occurs even if stresses exceed the failure criterion (Hantschel et al., 2012). As a result, unrealistic pore pressures may be allowed, especially for deeper zones in the basin.

6. Conclusion

For the areas with complex structural history, the reconstruction of pore pressure is a great challenge. This study highlights the important role of structural evolution in formation pressure in a compressional tectonic setting. By integrating structural history and BPSM, the 2D model provides a better understanding of how overpressure develops in response to vertical loading, horizontal compression, salt seal, faults and folds in a tectonically active basin.

The 2D modelling results indicate that main causes of overpressure vary with geologic time. Prior to 2.4 Ma, relatively weak overpressure developed dominantly due to disequilibrium compaction; from 2.4 Ma onward, horizontal compression has been becoming the main cause and results in strong overpressure. Strong overpressure develops mainly beneath the salt-bearing seal layer, and the magnitude of overpressure in northern part appears greater than southern part in the Kuqa Depression. Open faults prior to 1.75 Ma released overpressures in formations they passed through, releasing amount depending on formation permeability; closed faults since 1.75 Ma have divided the overpressured section into several pressure compartments. Folding leaded to groundwater-related overpressure (groundwater potential) near the land surface, and overpressure decreases with burial due to the topographic-driven flow.

The contribution of horizontal compression to overpressure is quantitatively evaluated using the poroelastic approach. The overpressure increment due to horizontal compression accounts for more than 60% of overpressure today, varying with lithology and deformation strength. Additionally, salt sensitivity analysis with a salt content of 30%–60% shows that an increase in salt leads to an earlier development of overpressure and significantly enhances the magnitude of overpressure in the underlying strata through reducing permeability of the seal rocks. This also indicates that sealing capacity is one of the main factors controlling overpressure development in the study area.

Declaration of competing interest

The authors declare that they have no known competing financial interests or personal relationships that could have appeared to influence the work reported in this paper.

Data availability

Data will be made available on request.

Acknowledgements

This study was cofounded by the National Nature Science Foundation of China (Grant No. U19B6003) and the Science and Technology Project from PetroChina Tarim Oilfield Company (Grant No. 041020050021). We thank PetroChina Tarim Oilfield Company for providing seismic and well data. We thank the editor and two anonymous reviewers for their constructive comments which helped to improve the manuscript.

References

Akrout, D., Cobbold, P.R., Ahmadi, R., Mercier, E., Montacer, M., 2016. Physical modelling of sub-salt gliding due to fluid overpressure in underlying sedimentary strata. Mar. Petrol. Geol. 72, 139–155. https://doi.org/10.1016/j.marpetgeo.2016.01.019.

Allan, U.S., 1989. Model for hydrocarbon migration and entrapment within faulted structures. AAPG (Am. Assoc. Pet. Geol.) Bull. 73, 803–811. https://doi.org/10.1306/44B4A271-170A-11D7-8645000102C1865D.

Allen, M.B., Vincent, S.J., Wheeler, P.J., 1999. Late cenozoic tectonics of the kepingtage thrust zone: interactions of the tien Shan and Tarim Basin, northwest China. Tectonics 18, 639–654. https://doi.org/10.1029/1999TC900019.

Allwardt, J.R., Michael, G.E., Shearer, C.R., Heppard, P.D., Ge, H.X., 2009. 2D modeling of overpressure in a salt withdrawal basin, Gulf of Mexico, USA. Mar. Petrol. Geol. 26, 464–473. https://doi.org/10.1016/j.marpetgeo.2009.01.009.

Athy, L.F., 1930. Density, porosity and compaction of sedimentary rocks. AAPG (Am. Assoc. Pet. Geol.) Bull. 14, 1–24. https://doi.org/10.1306/3D93289E-16B1-11D7-8645000102C1865D.

Barker, C., 1972. Aquathermal pressuring: role of temperature in development of abnormal pressure zone. AAPG (Am. Assoc. Pet. Geol.) Bull. 56, 2068–2071. https://doi.org/10.1306/819A41B0-16C5-11D7-8645000102C1865D.

Baur, F., Benedetto, M.D., Fuchs, T., Lampe, C., Sciamanna, S., 2009. Integrating structural geology and petroleum systems modeling–A pilot project from Bolivia's fold and thrust belt. Mar. Petrol. Geol. 26, 573–579. https://doi.org/10.1016/j.marpetgeo.2009.01.004.

Berry, F.A.F., 1973. High fluid potentials in California coast ranges and their tectonic significance. AAPG (Am. Assoc. Pet. Geol.) Bull. 57, 1219–1249. https://doi.org/10.1306/83D90E8A-16C7-11D7-8645000102C1865D.

Berthelon, J., Brüch, A., Colombo, D., Frey, J., Traby, R., Bouziat, A., Cacas-stentz, M.C., Cornu, T., 2021. Impact of tectonic shortening on fluid overpressure in petroleum system modelling: insights from the Neuquen basin, Argentina. Mar. Petrol. Geol. 127, 104933 https://doi.org/10.1016/j.marpetgeo.2021.104933.

Brown, J.P., Karim, R., 2008. Pore pressure prediction as a prospecting tool, input to risk, volumes and field development. In: AAPG Annual Convention. AAPG Memoir 76. AAPG, Texas, USA. https://doi.org/10.3997/2214-4609-pdb.258.GL15.

Burgreen-Chan, B., Meisling, K.E., Graham, S., 2016. Basin and petroleum system modelling of the East Coast Basin, New Zealand: a test of overpressure scenarios in a convergent margin. Basin Res. 28, 536–567. https://doi.org/10.1111/bre.12121.

England, W.A., Mackenzie, A.S., Mann, D.M., Quigley, T.M., 1987. The movement and entrapment of petroleum fluids in the subsurface. J. Geol. Soc. 144, 327–347. https://doi.org/10.1144/gsjgs.144.2.0327.

Fan, C.Y., Wang, G., Wang, Z.L., Han, X.J., Chen, J., Zhang, K.L., Zhang, B.S., 2021. Prediction of multiple origin overpressure in deep fold-thrust belt: a case study of Kuqa subbasin, Tarim Basin, northwestern China. AAPG (Am. Assoc. Pet. Geol.) Bull. 105, 1511–1533. https://doi.org/10.1306/01282119044.

Fisher, A.T., Zwart, G., 1996. Relation between permeability and effective stress along a plate-boundary fault, Barbados accretionary complex. Geology 24, 307–310. https://doi.org/10.1130/0091-7613(1996)024<0307:RBPAES>2.3.CO, 2.

Fu, X.F., Jia, R., Wang, H.X., Wu, T., Meng, L.D., Sun, Y.H., 2015. Quantitative evaluation of fault-caprock sealing capacity: a case from Dabei-Kelasu structural belt in Kuqa Depression, Tarim Basin, NW China. Petrol. Explor. Dev. 42, 329–338. https://doi.org/10.1016/S1876-3804(15)30023-9.

Gemmer, L., Ings, S.J., Medvedev, S., Beaumont, C., 2004. Salt tectonics driven by differential sediment loading: stability analysis and finite-element experiments. Basin Res. 16, 199–218. https://doi.org/10.1111/j.1365-2117.2004.00229.x.

Graham, S.A., Hendrix, M.S., Wang, L.B., Homewood, P., 1993. Collision successor basins of western China, impact of tectonic inheritance on sand composition. Geol. Soc. Am. Bull. 105, 323–344. https://doi.org/10.1130/0016-7606(1993)105<0323:CSBOWC>2.3.CO;2.

Grauls, D.J., Baleix, J.M., 1994. Role of overpressures and in situ stresses in fault-controlled hydrocarbon migration: a case study. Mar. Petrol. Geol. 11, 734–742. https://doi.org/10.1016/0264-8172(94)90026-4.

Guo, X.W., Liu, K.Y., Jia, C.Z., Song, Y., Zhao, M.J., Lu, X.S., 2016a. Effects of early petroleum charge and overpressure on reservoir porosity preservation in the giant Kela-2 gas field, Kuqa depression, Tarim Basin, northwest China. AAPG (Am. Assoc. Pet. Geol.) Bull. 100, 191–212. https://doi.org/10.1306/11181514223.

Guo, X.W., Liu, K.Y., Jia, C.Z., Song, Y., Zhao, M.J., Zhuo, Q.G., Lu, X.S., 2016b. Constraining tectonic compression processes by reservoir pressure evolution: overpressure generation and evolution in the Kelasu Thrust Belt of Kuqa Foreland Basin, NW China. Mar. Petrol. Geol. 72, 30–44. https://doi.org/10.1016/j.marpetgeo.2016.01.015.

Guo, X.W., Liu, K.Y., Jia, C.Z., Song, Y., Zhao, M.J., Lu, X.S., 2016c. Fluid evolution in the dabei gas field of the Kuqa depression, Tarim Basin, NW China: implications for fault-related fluid flow. Mar. Petrol. Geol. 78, 1–16. https://doi.org/10.1016/j.marpetgeo.2016.08.024.

Hantschel, T., Kauerauf, A.I., Wygrala, B., 2000. Finite element analysis and ray tracing modeling of petroleum migration. Mar. Petrol. Geol. 17, 815–820. https://doi.org/10.1016/S0264-8172(99)00061-6.

Hantschel, T., Kauerauf, A.I., 2009. Fundamentals of Basin and Petroleum Systems Modeling. Springer, Berlin.

Hantschel, T., Wygrala, B., Fuecker, M., Neber, A., 2012. Modeling basin-Scale geomechanics through geological time. In: International Petroleum Technology

Conference, 15-17 November, IPTC 15286. Bangkok, Thailand. https://doi.org/10.2523/IPTC-15286-MS.
Huang, W.K., Zeng, L.F., Pan, C.C., Xiao, Z.Y., Zhang, H.Z., Huang, Z.B., Zhao, Q., Yu, S., Xu, H., Chen, C.S., Liu, D.Y., Liu, J.Z., 2019. Petroleum generation potentials and kinetics of coaly source rocks in the Kuqa Depression of Tarim Basin, northwest China. Org. Geochem. 133, 32–52. https://doi.org/10.1016/j.orggeochem.2019.04.007.
Hubbert, M.K., Rubey, W.W., 1959. Role of fluid pressure in mechanics of overthrust faulting: I. Mechanics of fluid-filled porous solids and its application to overthrust faulting. Geol. Soc. Am. Bull. 70, 115–166. https://doi.org/10.1130/0016-7606(1959)70[115:ROFPIM]2.0.CO;2.
Jia, C., Li, Q.M., 2008. Petroleum geology of Kela-2, the most productive gas field in China. Mar. Petrol. Geol. 25, 335–343. https://doi.org/10.1016/j.marpetgeo.2008.01.002.
Li, M.J., Wang, T.G., Chen, J.F., He, F.Q., Yun, L., Akbar, S., Zhang, W.B., 2010. Paleo-heat flow evolution of the Tabei uplift in Tarim Basin, northwest China. J. Asian Earth Sci. 37, 52–66. https://doi.org/10.1016/j.jseaes.2009.07.007.
Li, S.Q., Wang, X., Suppe, J., 2012. Compressional salt tectonics and synkinematic strata of the western Kuqa foreland basin, southern Tian Shan, China. Basin Res. 24, 475–497. https://doi.org/10.1111/j.1365-2117.2011.00531.x.
Liang, D.G., Zhang, S.C., Chen, J.P., Wang, F.Y., Wang, P.R., 2003. Organic geochemistry of oil and gas in the Kuqa depression, Tarim Basin, NW China. Org. Geochem. 34, 873–888. https://doi.org/10.1016/S0146-6380(03)00029-9.
Lu, H.F., Jia, D., Chen, C.M., Cai, D.S., Wu, S.M., Wang, G.Q., Guo, L.Z., Shi, Y.S., 1997. Evidence for growth fault-bent folds in the Tarim Basin and its implications for fault-slip rates in the Mesozoic and Cenozoic. In: Structural Geology and Geomechanics Proceedings of the 30th International Geological Congress. IUGS, Boca Raton, Florida.
Luo, X.R., Vasseur, G., 1992. Contributions of compaction and aquathermal pressuring to geopressure and the influence of environmental conditions. AAPG (Am. Assoc. Pet. Geol.) Bull. 76, 1550–1559. https://doi.org/10.1306/BDFF8A42-1718-11D7-8645000102C1865D.
Luo, X.R., Vasseur, G., 1993. Contributions of compaction and aquathermal pressuring to geopressure and the influence of environmental conditions: reply. AAPG (Am. Assoc. Pet. Geol.) Bull. 77, 2011–2014. https://doi.org/10.1306/bdff8fb0-1718-11d7-8645000102c1865d.
Luo, X.R., Vasseur, G., 1995. Modelling of pore pressure evolution associated with sedimentation and uplift in sedimentary basins. Basin Res. 7, 35–52. https://doi.org/10.1111/j.1365-2117.1995.tb00094.x.
Luo, X.R., Vasseur, G., 1996. Geopressuring mechanism of organic matter cracking: numerical modeling. AAPG (Am. Assoc. Pet. Geol.) Bull. 80, 856–874. https://doi.org/10.1306/64ED88EA-1724-11D7-8645000102C1865D.
Maerten, L., Maerten, F., 2006. Chronologic modeling of faulted and fractured reservoirs using geomechanically based restoration: technique and industry applications. AAPG (Am. Assoc. Pet. Geol.) Bull. 90, 1201–1226. https://doi.org/10.1306/02240605116.
Mildren, S.D., Hillis, R.R., Fett, T., Robinson, P.H., 1994. Contemporary stresses in the Timor Sea: implications for fault-trap integrity. In: The Sedimentary Basins of Western Australia: Proceedings of the Petroleum Exploration Society of Australia Symposium, pp. 291–300.
Neumaier, M., Littke, R., Hantschel, T., Maerten, L., Joonnekindt, J.P., Kukla, P., 2014. Integrated charge and seal assessment in the Monagas fold and thrust belt of Venezuela. AAPG (Am. Assoc. Pet. Geol.) Bull. 98, 1325–1350. https://doi.org/10.1306/01131412157.
Nordgård-Bolås, H.M., Hermanrud, C., Teige, G.M.G., 2005. Seal capacity estimation from subsurface pore pressures. Basin Res. 17, 583–599. https://doi.org/10.1111/j.1365-2117.2005.00281.x.
O'Connor, D., Swarbrick, R., Jones, D., 2008. Where has all the pressure gone? Evidence from pressure reversals and hydrodynamic flow. First Break 26, 55–61. https://doi.org/10.3997/1365-2397.2008013.
Peters, K.E., Nelson, P.H., 2012. Criteria to determine borehole formation temperatures for calibration of basin and petroleum system models. SEPM (Soc. Sediment. Geol.) Spec. Publ. 103, 5–15.
Pi, X.J., Xie, H.W., Zhang, C., Tian, Z.J., 2002. Mechanisms of abnormal overpressure generation in Kuqa foreland thrust belt and their impacts on oil and gas reservoir formation. Chin. Sci. Bull. 47, 85–93. https://doi.org/10.1007/BF02902823.
Qin, S.F., Dai, J.X., Liu, X.W., 2007. The controlling factors of oil and gas generation from coal in the Kuqa Depression of Tarim Basin, China. Int. J. Coal Geol. 70, 255–263. https://doi.org/10.1016/j.coal.2006.04.011.
Qiu, N.S., Chang, J., Li, J.W., Li, W.Z., Yun, L., Li, H.L., 2012. New evidence on the Neogene uplift of South Tianshan: constraints from the (U–Th)/He and AFT ages of borehole samples of the Tarim basin and implications for hydrocarbon generation. Int. J. Earth Sci. 101, 1625–1643. https://doi.org/10.1007/s00531-011-0745-0.
Schlumberger, 1989. Log Interpretation Principles/applications. Schlumberger Manul, Houston, Texas.
Schultz-Ela, D.D., 1992. Restoration of cross-sections to constrain deformation processes of extensional terranes. Mar. Petrol. Geol. 9, 372–388. https://doi.org/10.1016/0264-8172(92)90049-K.
Shi, G.R., 2008. Basin modeling in the Kuqa depression of the Tarim Basin (western China): a fully temperature-dependent model of overpressure history. Math. Geosci. 40, 47–62. https://doi.org/10.1007/s11004-007-9133-5.
Swarbrick, R.E., 2002. Developing pressure histories through basin modeling. In: Annual Meeting Expanded Abstracts. AAPG & SEPM, Tulsa, Oklahoma, p. 171.
Swarbrick, R.E., Osborne, M.J., Yardley, G.S., 2002. Comparison of overpressure magnitude resulting from the main generating mechanisms. AAPG Memoir 76, 1–12.
Tang, L.J., Jia, C.Z., Jin, Z.J., Chen, S.P., Pi, X.J., Xie, H.W., 2004. Salt tectonic evolution and hydrocarbon accumulation of Kuqa foreland fold belt, Tarim Basin, NW China. J. Petrol. Sci. Eng. 41, 97–108. https://doi.org/10.1016/S0920-4105(03)00146-3.
Tang, X.Y., Yang, S.C., Hu, S.B., 2014. Thermal and maturation history of Jurassic source rocks in the Kuqa foreland depression of Tarim Basin, NW China. J. Asian Earth Sci. 89, 1–9. https://doi.org/10.1016/j.jseaes.2014.03.023.
Terzaghi, K., 1943. Theoretical Soil Mechanics. John Wiley, New York.
Tingay, M.R.P., Morley, C.K., Laird, A., Limpornpipat, O., Krisadasima, K., Pabchanda, Suwit, Macintyre, H.R., 2013. Evidence for overpressure generation by kerogen-to-gas maturation in the northern Malay Basin. AAPG (Am. Assoc. Pet. Geol.) Bull. 97, 639–672. https://doi.org/10.1306/09041212032.
Underschultz, J., Strand, J., 2016. Capillary seal capacity of faults under hydrodynamic conditions. Geofluids 16, 464–475. https://doi.org/10.1111/gfl.12166.
Ungerer, P., 1990. State of the art of research in kinetic modelling of oil formation and expulsion. Org. Geochem. 16, 1–25. https://doi.org/10.1016/0146-6380(90)90022-R.
Wan, J.L., Huang, W.H., Gong, Y.J., Zhuo, Q.G., Lu, X.S., 2021. Hydrocarbon accumulation process and mechanism in the lower Jurassic reservoir in the eastern Kuqa depression, Tarim Basin, northwest China: a case study of well Tudong 2 in the Tugerming area. ACS Omega 6, 30344–30361. https://doi.org/10.1021/acsomega.1c03421.
Wang, H., 2000. Theory of Linear Poroelasticity with Applications to Geomechanics and Hydrogeology. Princeton University Press, Princeton, New Jersey.
Wang, L.S., Li, C., Liu, S.W., Li, H., Xu, M.J., Yu, D.Y., 2005. Terrestrial heat flow distribution in Kuqa forelandbasin, Tarim, NW China. Petrol. Explor. Dev. 32, 79–83. https://doi.org/10.3321/j.issn:1000-0747.2005.04.013 (in Chinese with English abstract).
Wang, P.W., Pang, X.Q., Jiang, Z.X., Guo, Y.C., Chen, X., Wang, Y.W., Jiao, J., 2016. Origin and evolution of overpressure in the lower Jurassic succession in the Kuqa depression, western China. J. Nat. Gas Sci. Eng. 28, 700–710. https://doi.org/10.1016/j.jngse.2015.12.002.
Wang, Q.C., Zhang, Z.P., Lin, W., 2004. Late tertiary faults and their paleostress along the boundary between the Kuqa basin and the Tianshan mountains. Chin. Sci. Bull. 4, 374–381. https://doi.org/10.1007/BF02900321.
Wang, X., Suppe, J., Guan, S.W., Hubert-Ferrari, A., Gonzalez-Mieres, R., Jia, C.Z., 2011. Cenozoic structure and tectonic evolution of the Kuqa Foldbelt, southern Tianshan, China. AAPG Memoir 94, 215–243. https://doi.org/10.1306/13251339M94389.
Webster, M., O'conner, S., Pindar, B., Swarbrick, R., 2011. Overpressures in the Taranaki Basin: distribution, causes, and implications for exploration. AAPG (Am. Assoc. Pet. Geol.) Bull. 95, 339–370. https://doi.org/10.1306/06301009149.
Wygrala, B.P., 1989. Integrated Study of an Oil Field in the Southern Po Basin, Northern Italy. PhD Dissertation. University of Cologne, Germany.
Yang, S.M., Li, J., Wang, Q., 2008. The deformation pattern and fault rate in the Tianshan Mountains inferred from GPS observations. Sci. China (Ser. D: Earth Sci. 51 (8), 1064–1080. https://doi.org/10.1007/s11430-008-0090-8.
Yin, A., Nie, S., Craig, P., Harriso, T.M., Ryerson, F.J., Qian, X.L., Yang, G., 1998. Late Cenozoic tectonic evolution of the southern Chinese Tian Shan. Tectonics 17, 1–27. https://doi.org/10.1029/97TC03140.
Yu, H.B., Qi, J.F., Yang, X.Z., Sun, T., Liu, Q.Y., Cao, S.J., 2016. Analysis of mesozoic prototype Basin in Kuqa depression, Tarim Basin. Xinjing Pet. Geol. 37, 644–654 (in Chinese with English abstract).
Zeng, L.B., Liu, B.M., 2006. Abnormal high pressure in Kuqa foreland thrust belt of Tarim basin: origin and impacts on hydrocarbon accumulation. Prog. Nat. Sci. 16, 1307–1314. https://doi.org/10.1080/10020070612330146.
Zeng, L.B., Wang, H.J., Gong, L., Liu, B.M., 2010. Impacts of the tectonic stress field on natural gas migration and accumulation: a case study of the Kuqa Depression in the Tarim Basin, China. Mar. Petrol. Geol. 27, 1616–1627. https://doi.org/10.1016/j.marpetgeo.2010.04.010.
Zhang, F.Q., Lu, X.S., Botterill, S., Gingras, M., Zhuo, Q.G., Zhong, H.L., 2021. Horizontal tectonic stress as a cause of overpressure in the southern margin of the Junggar Basin, northwest China. J. Petrol. Sci. Eng. 205, 108861 https://doi.org/10.1016/j.petrol.2021.108861.
Zhao, W.Z., Zhang, S.C., Wang, F.Y., Cramer, B., Chen, J.P., Sun, Y.G., Zhang, B.M., Zhao, M.J., 2005. Gas systems in the Kuche Depression of the Tarim Basin: source rock distributions, generation kinetics and gas accumulation history. Org. Geochem. 36, 1583–1601. https://doi.org/10.1016/j.orggeochem.2005.08.016.
Zhou, X.X., 2001. The mesozoic-cenozoic fluid pressure structure and reservoir-forming machine process in the Kuqa petroleum system in the Tarim basin. Earth Sci. Front. 8, 351–361.
Zhu, G.Y., Wang, H.T., Weng, N.A., Yang, H.J., Zhang, K., Liao, F.R., Neng, Yuan, 2015. Geochemistry, origin and accumulation of continental condensate in the ultra-deep-buried Cretaceous sandstone reservoir, Kuqa Depression, Tarim Basin, China. Mar. Petrol. Geol. 65, 103–113. https://doi.org/10.1016/j.marpetgeo.2015.03.025.
Zhuo, Q.G., Meng, F.W., Song, Y., Yang, H.J., Li, Y., Ni, P., 2014. Hydrocarbon migration through salt: evidence from Kelasu tectonic zone of Kuqa foreland basin in China. Carbonates Evaporites 29, 291–297. https://doi.org/10.1007/s13146-013-0177-y.
Zoback, M., 2007. Reservoir Geomechanics. Cambridge University Press, New York.